A PHYSIOLOGICALLY-BASED, PHARMACOKINETIC MODEL FOR THE CLEARANCE OF PEGYLATED NANOMEDICINES

Anne M. Talkington

A dissertation submitted to the faculty at the University of North Carolina at Chapel Hill in partial fulfillment of the requirements for the degree of Doctor of Philosophy in the Curriculum of Bioinformatics and Computational Biology.

Chapel Hill
2021

Approved by:

M. Gregory Forest

Samuel K. Lai

Yanguang Cao

Kathleen M. Caron

Timothy C. Elston

ABSTRACT

Anne M. Talkington: A Physiologically-Based, Pharmacokinetic Model for the Clearance of PEGylated Nanomedicines
(Under the direction of M. Gregory Forest and Samuel K. Lai)

Physiologically-based pharmacokinetic (PBPK) models are valuable for conducting large-scale *in silico* experiments to assist in various stages of drug development, including determining optimal dosing strategies, modifying these strategies for special populations, or testing different applications for therapeutics. In doing so, PBPK serves as an alternative for time-consuming, costly, and potentially unethical *in vivo* experiments or clinical trials: it can be used to predict and optimize the success of proposed treatments using known (well-determined physiologically) or learned (through experiments or data-driven analyses) kinetics of the system mimicking complex human physiology. In turn, PBPK modeling can enable more efficient design and optimization of *in vivo* experiments, thus accelerating pre-clinical screening and development of therapeutics. In this thesis, I discuss the application of PBPK modeling to an important problem in the medical community – the accelerated clearance of PEGylated drugs in the presence of anti-PEG antibodies (APA). For example, Krystexxa, a PEGylated uricase used to treat severe chronic gout, is ineffective in approximately half of patients, and 5% of the patients experience severe hypersensitivity, including anaphylaxis, as a result of APA.

Here I present a multi-compartment PBPK model to accurately predict the biodistribution and clearance behavior of PEGylated liposomal drug carriers, and validate the model predictions against drug biodistribution data obtained via PET/CT technology. I then analyze the model to

identify mechanistic behaviors underlying APA-mediated accelerated clearance using parameter estimation and optimization techniques, namely Latin Hypercube Sampling. Finally, I demonstrate that pre-injection with a high molecular weight free PEG effectively restores plasma Krystexxa levels to a naïve-like biodistribution in mice with clinical levels of APA, suggesting a potential strategy for mitigating the accelerated blood clearance (ABC) effect in the clinic. In considering such a translation, PBPK modeling is a powerful tool that holds the potential to suggest further optimization of our strategy to mitigate ABC.

To my family and friends – thank you for your unending support.

PREFACE

In this dissertation, I present a body of work on the biodistribution patterns of PEGylated nanomedicines, which I explore both experimentally and computationally. First, I present a multi-compartment physiologically-based pharmacokinetic (PBPK) model for PEGylated liposomes (PL) and how anti-PEG antibodies (APA) alter the biodistribution and PK profile of PEGylated liposomal drugs. APA are responsible for the accelerated clearance of drug from the bloodstream. The model recapitulates and predicts this accelerated blood clearance (ABC) behavior at both short (1 hour of high temporal resolution) and long timescales (96h). These predictions have been validated against continuous-scan PET/CT data in cohorts of APA-sensitized and naïve mice.

I then present an analysis of the 8-compartment PBPK model, in which I demonstrate the use of parameter estimation and optimization techniques to explore the parameter space for values that have not been well-documented. Implementing a Latin Hypercube Sampling algorithm reveals uncertainty and variability in parameter space, which indicates which parameters in the model are most responsible for the clearance behavior of the PL. Leveraging this knowledge, we can begin to understand the primary mechanisms responsible for ABC at a level we are unable to investigate experimentally. Namely, we identify and quantify increased liver retention of PL, which occurs when APA bind to Fc receptors in the liver. Increased retention in the spleen is significantly involved as a secondary mechanism. No changes to extravasation, or tissue permeability, were detected between the naïve and APA+ cohorts.

Finally, given the experimental data and PBPK model-based analysis of ABC, I propose and test a method to mitigate the effect. Building off of promising results from previous studies in our lab, I tested a pre-injection of high molecular weight (MW) free PEG prior to a second dose in mice sensitized to Krystexxa, a PEGylated uricase. The results of this study demonstrate the potential to alleviate APA-mediated clearance. Mice with low APA titers saw full or near full recovery of the area under the curve (AUC) in the plasma at 96h, and even moderate to high APA levels saw 3-fold increase in plasma AUC at 96h relative to mice that did not receive the PEG intervention. This suggests the ability to significantly increase the circulation time of PEGylated therapeutics in the presence of APA.

Together, this work suggests a deeper mechanistic understanding and possible mechanisms for alleviating ABC as a result of APA. Furthermore, our PBPK model has demonstrated its potential as a predictive tool in developing drugs and response to anti-drug antibodies.

This dissertation contains preprints of work that have been submitted to the Bulletin of Mathematical Biology, regarding the parameterization of PBPK models, and the Journal of Controlled Release, regarding the development of PBPK models for PEGylated nanomedicines and free PEG intervention. Funding for the work presented in each chapter is as follows:

Chapter 1:

This work was supported by The David and Lucile Packard Foundation (2013-39274, SKL), National Institutes of Health (T32-HL069768 for AMT; R01HL141934 for SKL; R35GM119661 for YC), P.E.O. International (AMT), and Eshelman Institute of Innovation

(SKL). MGF and TW were supported in part from the National Science Foundation (NSF) grants DMS-1664645, DMS-2028758, CISE-1931516.

Chapter 2:

This work was supported by The David and Lucile Packard Foundation (2013-39274, SKL), National Institutes of Health (T32-HL069768, AMT; HL141934, SKL; R35GM119661, YC), P.E.O. International (AMT), and an Eshelman Institute of Innovation award (SKL). MGF was supported in part from the National Science Foundation (NSF) DMS-1517274, DMS-1664645, DMS-1816630.

Chapter 3:

This work was supported by The David and Lucile Packard Foundation (2013-39274, SKL), National Institutes of Health (T32-HL069768; AMT, R01 HL141934; SKL), P.E.O. International (AMT), and Eshelman Institute of Innovation (SKL). The BRIC Small Animal Imaging (SAI) core facility and UNC Lineberger Animal Core are supported in part by an NCI Grant P30-CA016086. The PET/CT equipment is supported by the NIH shared instrumentation grant (1S10OD023611, ZL).

TABLE OF CONTENTS

LIST OF TABLES

LIST OF FIGURES

LIST OF ABBREVIATIONS

ABC	Accelerated blood clearance
APA	Anti-PEG antibodies
ADA	Anti-drug antibodies
AUC	Area under the curve
LHS	Latin Hypercube Sampling
MW	Molecular weight
ODE	Ordinary differential equation
PBPK	Physiologically based pharmacokinetic
PEG	Polyethylene glycol
PET	Positron Emission Tomography
PK	Pharmacokinetics
PL	PEGylated liposomes

CHAPTER 1: A PBPK MODEL THAT RECAPITULATES ANTI-PEG ANTIBODY-MEDIATED ACCELERATED BLOOD CLERANCE OF PEGYLATED NANOMEDICINES IN VIVO[1]

Summary

PEGylation is routinely used to extend the systemic circulation of various protein therapeutics and nanomedicines. Nonetheless, mounting evidence is emerging that individuals exposed to select PEGylated therapeutics can develop antibodies specifically to PEG, i.e., anti-PEG antibodies (APA). In turn, APA increase both the risk of hypersensitivity to the drug as well as potential loss of efficacy due to accelerated blood clearance of the drug. Despite the broad implications of APA, the temporal dynamics with which APA can alter the pharmacokinetics and biodistribution of PEGylated drugs remain not well understood. Here, we report a physiologically based pharmacokinetic (PBPK) model that resolves both early- and late-phase pharmacokinetics and biodistribution of intravenously administered PEG-liposomes in the liver, spleen, lung, muscle, and kidney of mice with APA. The model accurately recapitulates PK and biodistribution data obtained from PET/CT imaging of radiolabeled PEG-liposomes. This PBPK model is readily adaptable to describe antibody-mediated clearance of other drugs, particles, and viruses, providing a powerful tool for predicting the pharmacokinetic impacts of anti-drug antibodies and the temporal dynamics with which antibodies can mediate clearance of foreign entities.

[1] This chapter is adapted from a preprint of an article submitted to the Journal of Controlled Release. The original citation is as follows:
Talkington A.M., McSweeney M.D., Wessler T., Rath M.K., Li Z., Zhang T., Yuan H., Frank J.E., Forest M.G., Cao Y., Lai S.K. "A PBPK model that recapitulates anti-PEG antibody-mediated accelerated blood clearance of PEGylated nanomedicines *in vivo*," Journal of Controlled Release (submitted).

Introduction

Polyethylene glycol (PEG) is an uncharged, hydrophilic polymer routinely used to increase the circulation time and decrease the immunogenicity of therapeutic drugs, especially highly immunogenic drugs that are susceptible to induction of **anti-drug antibodies (ADA)** [1]. The hydrophilicity of PEG increases the aqueous solubility of hydrophobic drugs, thereby improving stability and reducing aggregation [2-6]. In addition, the highly flexible nature of PEG sterically hinders the adsorption of opsonic proteins and other blood components, diminishes interactions with the immune system, increases hydrodynamic diameter, and reduces enzymatic degradation [3, 7]. The resulting 'stealth' effect greatly prolongs the systemic **pharmacokinetic (PK)** profiles of PEGylated therapeutics, sparing millions of patients from daily or weekly injections.

Unfortunately, over the past 15 years, it is increasingly shown that some patients can produce high titers of antibodies directed to PEG itself [8], a phenomenon likely enhanced by the immunogenicity of the underlying drug [9, 10]. We previously found detectible levels of anti-PEG antibodies (APA) in nearly 70% of blood samples from the general population [11], with the vast majority of subjects possessing an IgG isotype that implies the presence of immune memory and the possibility of rapid induction of APA. This is consistent with clinical observations that showed a sizable fraction of patients could develop APA when exposed to select PEGylated drugs. For instance, roughly one-third of pediatric acute lymphoblastic leukemia (ALL) patients developed APA that quickly eliminated Oncospar (PEG-asparaginase) from the circulation [12]. The incidence rate increases to nearly half of the patients treated with Krystexxa (PEG-uricase) [13-15], and can be even higher (as high as 100%) in patients treated with Palynziq (PEGylated phenylalanine ammonia lyase, or PEG-PAL) [16]. At sufficient titers,

APA can mediate **accelerated blood clearance (ABC)** of PEGylated drugs [17-23], likely by uptake of APA immune complexes by Kupffer cells and liver sinusoidal endothelial cells (LSEC) [20, 24]. APA also increases the frequency of hypersensitivity to PEGylated therapeutics [25, 26], as reflected by a range of allergic reactions, including anaphylactic shock, to pegloticase [27, 28], pegnivacogin [29], and PEG-containing products such as osmotic laxatives and cosmetic products [30]. More recently, APA is implicated in an allergic response to the Pfizer/BioNTec mRNA vaccines for SARS-CoV-2, due to the inclusion of PEG-lipids in its formulation [31, 32]. Despite the important implications of APA, the relationship between the circulating APA titers and the resulting impact on PK and biodistribution has not been established with high temporal resolution in the context of PK modeling.

Physiologically-based pharmacokinetic (PBPK) modeling is a powerful tool enabling a deeper understanding of the fate of drugs and drug carriers in complex biological environments. PBPK models can inform preclinical *in vivo* testing, and serve as a crucial tool to guide clinical evaluations as well as potential dosing regimens in special populations [33, 34]. Not surprisingly, PBPK models are routinely used to predict and interpret drug tissue distribution and clearance in various therapeutic areas, clinical scenarios, and patient populations [35, 36]. Many PBPK models recapitulating antibodies as biotherapeutics have been developed [37, 38]; however, fewer models exist that capture how endogenous ADA can alter the PK and biodistribution of the drugs. Previously, we developed a 2-compartment minimal PBPK model that captures APA-mediated accelerated blood clearance of **PEG-liposomes (PL)** [39, 40]. While useful in predicting the PK of PEGylated drugs over long timescales, the model was unable to reveal APA's impact on either biodistribution or early phase clearance of PEGylated drugs. In this work, we thus sought to develop a more comprehensive PBPK model that captures potential

APA-mediated clearance of PEGylated drugs to major organs (Figure 1.1). Leveraging high-resolution PET/CT scans of radiolabeled PEG-liposomes performed immediately following dosing to PEG-sensitized vs. naïve animals, we were able to verify that our PBPK model can accurately recapitulate the systemic PK and biodistribution of PEG-liposomes to liver, spleen, lung, kidney, and muscle in naïve and APA+ mice with high temporal resolution.

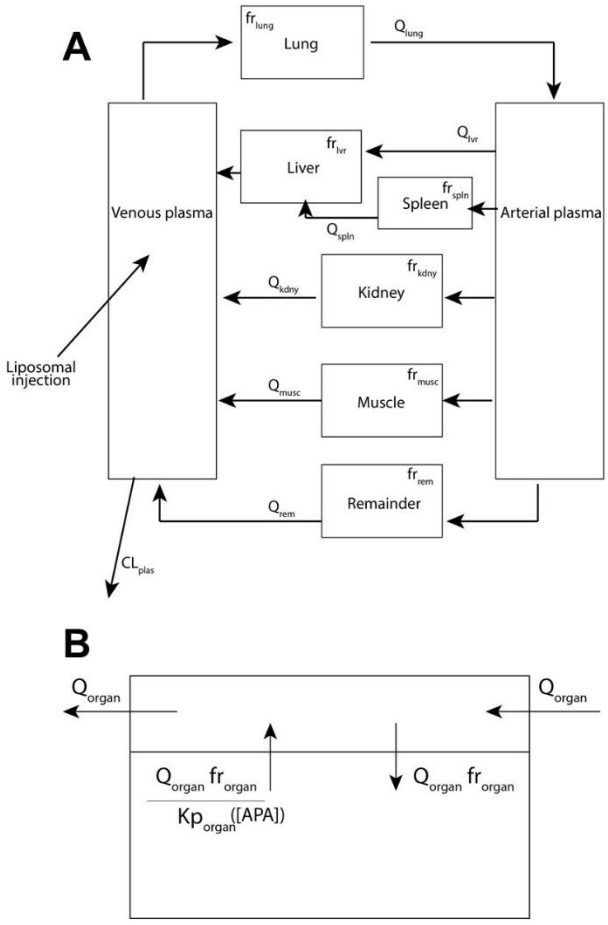

Figure 1.1. Schematic of the Model. (A) Schematic diagram of the PBPK model. (B) Illustration of PK within each organ compartment.

Materials & Methods

Production of empty PEG-liposomes (PL) for APA-induction

The PL used for induction were composed of phosphatidylcholine, cholesterol, and methoxy-PEG 2000 DSPE at a molar ratio of 39:56:5 [41]. The lipids were dissolved in a 2:1 chloroform: methanol solution in a glass vial, and evaporated with nitrogen gas to form a thin film. This film was desiccated overnight. The following day, PBS heated to 50 ^{o}C was added to the vial, which was sonicated at 15 30-second intervals. The liposomes in PBS solution were then extruded 9 times each at a controlled temperature of 50 ^{o}C through 400 nm and 100 nm filters. The liposomes were characterized with a Malvern Zetasizer Nano ZS (Malvern Instruments, Malvern, UK) via intensity PSD and confirmed to be 130 nm in diameter with PDI < 0.2.

Induction of APA in immunocompetent BALB/c mice

Female and male BALB/c mice (Charles River Labs) aged 4-5 weeks were used in this study. Animal procedures used in this study were approved by the University of North Carolina at Chapel Hill Institutional Animal Care and Use Committee. All mice were housed in non-sterile cages with constant access to food and water. To induce APA, mice were intravenously dosed with 150 µL (0.1 µmol lipids/kg bodyweight at 6 mL/kg) of PL in sterile PBS on Day 0, or 7 days prior to PET/CT imaging studies; APA-naïve mice (negative control) received PBS alone. On Day 6, a mandibular bleed was performed on each mouse. 200 µL whole blood was transferred in EDTA tubes on ice. The blood was centrifuged at 2000 rcf for 15 minutes to separate the plasma. Samples were stored at 4 ^{o}C prior to ELISA assay and moved to -80 ^{o}C for

long-term storage. IgG and IgM APA in the plasma were quantified via competition ELISA, following the methods described previously [40] (Table 1.1).

Quantitation of APA titers

We determined the concentration of IgG and IgM APA via competition ELISA, run in duplicate for reproducibility. 96-well plates (Corning Costar 3695) were coated with DSPE-PEG5000 and stored overnight at 4 ^{o}C. They were then blocked for 1 hour at room temperature with 5% milk in 1x PBS. Plasma samples were diluted 50-fold and 400-fold in 1% milk, and tested in duplicate wells. Competition wells consisted of plasma at 50- or 400- fold dilution in 1% milk with 8 kDa PEG. The standard curve consisted of serial dilutions of mouse anti-PEG IgG (Silver Lake, CH2076) and IgM (Academia Sinica, AGP4 (AGP4-PABM-A)). After overnight incubation at 4 ^{o}C, goat anti-mouse IgG (Invitrogen, A28177, lot TG2596484) or IgM (ThermoFisher Life Technologies, 626820, lot QB215229) conjugated to HRP was added to the wells. The plates were incubated for 1 hour at room temperature. The color change was initiated by TMB and stopped with 1N HCl, and absorbance was measured at 450 and 570nm. IgG and IgM concentrations were calculated based on 5-parameter logistic regression on the standard curve rows. The ELISA assays sensitively detected APA levels in excess of 0.6 µg/mL IgG and 0.2 µg/mL IgM. IgG and IgM APA below this level did not lead to appreciable accelerated blood clearance of PEG-liposomes [40].

Preparation of radio-labeled PL for PET/CT imaging

PL with terminal amine groups on its PEG chains were obtained from Encapsula NanoSciences, and comprised of Hydrogenated Soy Phosphatidylcholine: cholesterol: DSPE-PEG(2000): DSPE-PEG(2000)-Amine at a molar ratio of 57:38:4:1 (lots IMS2007-08272019, IMS2007-04162019, and IMS2007-07212020). The liposomes were radiolabeled with ^{64}Cu chelated with DOTA or ^{89}Zr chelated with Df (p-SCN-Bn-deferoxamine lot B70510004-150407) at 0.5% exposed amine groups [42]. Purification studies for the first scan group were conducted using a 30 kDa spin filter and produced 40-60% yield. The signal of the product was still sufficient through 48h, far longer than the initial phase of interest for this study. Purification for the second scan group was conducted using a PD-10 column and resulted in up to approximately 90% yield, even after 24 hours. The stability of the labeling was approximately 90%. Purification for the third scan group resulted in approximately 67% yield with 24-hour stability of approximately 70%.

PET/CT Imaging

On day 7, mice underwent PET/CT imaging with radiolabeled PL. Naïve and APA+ mice (n=6 for each cohort) were imaged. The mice were scanned in three groups of four mice each, with n=2 from each cohort in each scan group (Table 1.2). Imaging was performed using a small animal PET/CT scanner (SuperArgus_4R, Sedecal, Inc. Spain). Mice were anesthetized with inhalation of 1.5%-2.5% isoflurane-oxygen gas mixture. Radiolabeled PL (5~7 MBq, estimated ~2.1 µmol of PL) was administrated through tail vein catheter, followed immediately by a 60 min dynamic PET scan. CT was conducted for anatomical reference and attenuation correction. Repeated PET/CT imaging (~20 min of PET acquisition) was conducted at 3, 24, and 48 hours

post the injection of radiolabeled PL. After the final imaging, major organs were collected and weighed, and radioactivity was further measured using a gamma counter to verify PET/CT results.

PET images were reconstructed using the 3D-OSEM algorithms with scatter, attenuation, and decay correction. Standardized uptake value (SUV) was calculated voxel-wise by normalizing the signal to the injection dose and animal body weight. Image analysis was conducted using PMOD software (version 3.9). Regions of interest (ROI) were delineated based on fused PET/CT images, and the uptake level of each ROI was reported in mean %ID/g.

Table 1.1. APA titer and weight for mice in study.

Mouse #	**51**	**52**	**56**	**57**	**545**	**546**	**547**	**548**	**974**	**981**	**984**	**982**
IgG APA (ug/mL)	-	37	-	63	-	-	>100	33	-	16	-	30
Total Weight (g)	22.7	22	15.6	17.7	21.8	21.4	22.1	21	22.2	20.1	19.9	18

Table 1.2. Parameters fit to each mouse in the study.

	Group 1				Group 2				Group 3			
Mouse #	**51**	**52**	**56**	**57**	**545**	**546**	**547**	**548**	**974**	**981**	**984**	**982**
fr_{lvr}	0.1131	0.0675	0.092	0.057	0.0992	0.0827	0.0592	0.0848	0.0998	0.093	0.0958	0.0665
fr_{kdny}	0.1876	0.0851	0.1936	0.1081	0.1956	0.1787	0.2037	0.1994	0.1962	0.1327	0.1463	0.1371
fr_{spln}	0.0701	0.0998	0.0545	0.0504	0.0502	0.05	0.0527	0.0867	-	-	-	-
fr_{musc}	0.0715	0.0107	0.0258	0.013	0.0399	0.0305	0.04	0.0351	0.0332	0.0311	0.0367	0.0341
fr_{lung}	0.1356	0.0501	0.1066	0.1056	0.0689	0.09	0.1917	0.0962	0.1406	0.1509	0.1545	0.1529
fr_{rem}	0.1481	0.0693	0.1958	0.0329	0.1028	0.1359	0.0402	0.1182	0.1258	0.1015	0.1237	0.0818
Kp_{lvr}	0.4419	2.5	0.4352	1.8686	0.5126	0.5048	2.7446	3.7439	0.7336	2.7909	0.62	2.7491
Kp_{kdny}	0.3081	0.3789	0.23	0.2302	0.2255	0.2119	0.3245	0.3532	0.16	0.3017	0.2022	0.35
Kp_{spln}	0.4132	1.8672	0.45	0.6138	0.4843	0.43	1.0947	1.8447	-	-	-	-
Kp_{musc}	0.0314	0.0208	0.04	0.0135	0.0632	0.06	0.0297	0.0243	0.0131	0.0085	0.0139	0.0101
Kp_{lung}	0.479	0.5213	0.3858	0.501	0.3953	0.3648	0.3327	0.6029	0.5896	0.467	0.5079	0.3583
Kp_{rem}	0.0105	0.0107	0.009	0.0119	0.0113	0.0114	0.0101	0.01	0.0102	0.0113	0.0091	0.0097
CL_{plas}	0.0068	0.0059	0.0035	0.0113	0.0119	0.009	0.0125	0.002	0.0144	0.0216	0.018	0.0067

PBPK Model

A system of Ordinary Differential Equations (ODEs) was developed to describe the physiologically-based pharmacokinetic system (Figure 1.1, Eqns 1-8). Each organ was treated as a well-stirred compartment, and drug transfer from blood to tissue was assumed to follow Fick's law of diffusion. A remainder compartment was considered to maintain the mass balance of drugs in the system. Tissue distribution rate was primarily restricted by liposomes' vascular permeability due to their approximately 100 nm (80-130 nm) size. The average concentration vs. time profiles in each compartment were reported. As the liposomes were too large to reach the deep tissue cellular layers, the radioactivity signal primarily originated from the vascular and interstitial sub-compartments. Transfer between compartments was driven by blood flow. The

amount of drug reaching and being retained by each organ was adjusted by perfusion and permeability coefficients.

$$\frac{dDrug_{plas}}{dt} = 1/V_{plas} \cdot \left(-Drug_{plas} \cdot CL_{plas}\right) - Qt_{lung} \cdot fr_{lung} \cdot Drug_{plas}/V_{plas} + \left(Qt_{lvr} \cdot fr_{lvr} + Qt_{spln} \cdot fr_{spln}\right)/V_{plas} \cdot \left(Drug_{lvr}/Kp_{lvr}\right) + Qt_{musc} \cdot fr_{musc}/V_{plas} \cdot \left(Drug_{musc}/Kp_{musc}\right) + Qt_{kdny} \cdot fr_{kdny}/V_{plas} \cdot \left(Drug_{kdny}/Kp_{kdny}\right) + Q_{rem} \cdot fr_{rem}/V_{plas} \cdot \left(Drug_{rem}/Kp_{rem}\right) \quad (1)$$

$$\frac{dDrug_{lvr}}{dt} = 1/V_{\ \ lvr} \cdot \left(Qt_{lvr} \cdot fr_{lvr} \cdot Drug_{art} - \left(Qt_{lvr} \cdot fr_{lvr} + Qt_{spln} \cdot fr_{spln}\right) \cdot Drug_{lvr}./Kp_{lvr}\right) + Qt_{spln} \cdot fr_{spln}/V_{\ \ lvr} \cdot \left(Drug_{spln}/Kp_{spln}\right) - Drug_{lvr}/(Kp_{lvr} \cdot V_{\ \ lvr}) \cdot CL_{lvr} \quad (2)$$

$$\frac{dDrug_{kdny}}{dt} = Qt_{kdny} \cdot fr_{kdny}/V_{\ \ kdny} \cdot \left(Drug_{art} - Drug_{kdny}/Kp_{kdny}\right) - Drug_{kdny}/\left(Kp_{kdny} \cdot V_{\ \ kdny}\right) \cdot CL_{kdny} \quad (3)$$

$$\frac{dDrug_{spln}}{dt} = Qt_{spln} \cdot fr_{spln}/V_{\ \ spln} \cdot \left(Drug_{art} - Drug_{spln}/Kp_{spln}\right) \quad (4)$$

$$\frac{dDrug_{musc}}{dt} = Qt_{musc} \cdot fr_{musc}/V_{\ \ musc} \cdot \left(Drug_{art} - Drug_{musc}/Kp_{musc}\right) \quad (5)$$

$$\frac{dDrug_{art}}{dt} = Qt_{lung} \cdot fr_{lung}/V_{art} \cdot \left(Drug_{lung}/Kp_{lung}\right) - Drug_{art} \cdot (Qt_{lvr} \cdot fr_{lvr}/V_{art} + Qt_{musc} \cdot fr_{musc}/V_{art} + Qt_{spln} \cdot fr_{spln}/V_{art} + Qt_{kdny} \cdot fr_{kdny}/V_{art} + Q_{rem} \cdot fr_{rem}/V_{art}) \quad (6)$$

$$\frac{dDrug_{lung}}{dt} = Qt_{lung} \cdot fr_{lung} \cdot Drug_{plas}/V_{\ \ lung} - Qt_{lung} \cdot fr_{lung} \cdot Drug_{lung}/\left(V_{\ \ lung} \cdot Kp_{lung}\right) \quad (7)$$

$$\frac{dDrug_{rem}}{dt} = Q_{rem} \cdot fr_{rem}/V_{rem} \cdot \left(Drug_{art} - Drug_{rem}/Kp_{rem}\right) \quad (8)$$

All physiological parameters, including the blood flows and tissue volumes, were taken from the literature (Table 1.3) [38, 43-45]. The interstitial tissue volume (V_{organ}) values were obtained by subtracting the respective vascular plasma contribution from the total organ volume (Table 1.3). For example, $V_{lvr} = (1 - PlasFracV_{lvr}) \times V_{lvr}^{whole}$. The initial values of the partitioning coefficients (Kp_{tissue}) were determined by taking the ratio of area under the curve (AUC) between tissue and plasma, which were then optimized (Table 1.2) [46]. The apparent permeability coefficients of liposomes across vascular membrane were also optimized, accounting for the intrinsic permeability and the impact of other variables at *in vivo* conditions (shear stress, osmotic pressure, etc.) (Table 1.2). Initial conditions were determined from the peaking time of tissue profiles in the data. The model was initialized at the point at which the total PET signal stabilized in the mouse, at approximately 1-minute post-injection. The system was solved numerically using MATLAB's ode15s function (MATLAB R2019a). The PET data for each organ included total signal from both the tissue and residual blood plasma. Therefore, when comparing the model output to the data, we computed a weighted average of PL contained in each organ's tissue and plasma. Parameters were optimized to obtain individual fits for each mouse using Latin Hypercube Sampling (Table 1.2) [47, 48].

Table 1.3. Physiological parameters in the PBPK model in 20 g mice.

Parameter	**Interpretation**	**Value**	**Ref**
Qt_{lvr}	Plasma flow through liver (mL/min)	1.1	[38]
Qt_{kdny}	Plasma flow through kidney (mL/min)	0.8	[38]
Qt_{spln}	Plasma flow through spleen (mL/min)	0.05	[38]
Qt_{musc}	Plasma flow through muscle (mL/min)	0.8	[38]
Qt_{lung}	Plasma flow through lung (mL/min)	4.38	[38]
V_{lvr}^{whole}	Volume of liver	1.75	[43, 44]
V_{kdny}^{whole}	Volume of kidney	0.32	[43, 44]
V_{spln}^{whole}	Volume of spleen	0.1	[43, 44]
V_{musc}^{whole}	Volume of muscle	7.6	[43, 44]
V_{lung}^{whole}	Volume of lung	0.12	[43, 44]
V_{plas}	Volume of venous blood plasma (mL)	0.67	[45]
V_{art}	Volume of arterial blood plasma (mL)	0.67	[45]
$PlasFracV_{lvr}$	Fraction of volume of murine liver comprised of plasma	0.155	[43, 45]
$PlasFracV_{kdny}$	Fraction of volume of murine kidney comprised of plasma	0.120	[43, 45]
$PlasFracV_{spln}$	Fraction of volume of murine spleen comprised of plasma	0.085	[43, 45]
$PlasFracV_{musc}$	Fraction of volume of murine muscle comprised of plasma	0.020	[43, 45]
$PlasFracV_{lung}$	Fraction of volume of murine lung comprised of plasma	0.250	[43, 45]

Results

PET/CT imaging reveals APA quickly eliminates PEG-liposomes from the circulation

In our previous study that relied on quantifying doxorubicin levels in the blood and different organs collected from sacrificed animals, we were unable to gain insights into the PK and biodistribution of Doxil® between 5 mins and 3 hours post-infusion. In contrast, PET/CT imaging, by tracking the PK and biodistribution of radiolabeled entities in the same mouse in nearly continuous time, can accurately reveal the physiological fate of drugs and drug carriers with unparalleled temporal resolution even with just a small number of animals (Figure 1.2A). To investigate the temporal dynamics with which APA can mediate clearance of PEGylated drug carriers, we thus performed PET/CT imaging in naïve and PEG-sensitized mice infused with radiolabeled PEG-liposomes.

All mice exhibited a rapid initial re-distribution of PL signals within the first minute of infusion. Naïve mice then exhibited very little change in plasma PL over the first hour, retaining ~50% of the total signal (i.e., injected dose) (Figure 1.2B). Of the remaining 50% of the PL radioactivity, ~30% was found in the liver, with a steady level observed throughout the first hour of the scan. Muscle mass comprised ~10-20% of the total signal, but was generally very noisy and reflected low, diffuse concentrations. Roughly 1% of the signal was present in the spleen, ~2.5% in the lung, and ~3-4% in the kidney at 1 h after dosing. The trends in change in radioactivity signal over time for the lung and kidney mirrored those in the blood, whereas the trends in the spleen mirrored those in the liver, with much of the increase found within the first 10 minutes post-infusion. These results are consistent with PL distribution primarily to the plasma sub-compartments for each tissue immediately following intravenous dosing, followed by gradual extravasation to the organ interstitium. The difference in the trend of radioactivity

accumulation over time likely relates to different rates of extravasation and immune cell uptake in the different organs.

In contrast, PL-sensitized mice with substantial APA titers exhibited rapid and extensive clearance of PL from the systemic circulation within the first hour post-infusion, retaining only ~20% of the injected dose in the circulation at the end of the first hour, less than half of the signal measured in the naïve mice. Much of the clearance from the systemic circulation appeared to occur within the first 10-15 minutes. We found a corresponding increase in PL radioactivity in the liver over the same time frame, accounting for nearly 75% of the injected dose. The dominant hepatic accumulation is consistent with APA-mediated clearance by Kupffer cells and LSECs. In contrast, the spleen, the lung, and the kidney retained only ~2%, ~1%, and ~2.5% of the PL-associated radioactivity at the end of the first hour. The difference in the measured radioactivity by the end of the first hour translates to statistically significant differences in the AUC in the plasma and liver between naïve and PL-sensitized, APA+ mice even within such short duration ($p < 0.001$, Welch's t-test) (Figure 1.2C).

Unfortunately, by 24 hrs post-infusion, we were unable to detect appreciable radioactivity in the heart from PET/CT imaging (data not shown), which is far shorter than the half-life of PL such as Doxil® established from earlier studies [40]. We believe this is unlikely due to the natural decay in radioactivity of ^{64}Cu, as we were also unable to detect a signal from PL labeled with ^{89}Zr. Instead, the most likely explanation is that the amine-functionalized PL preparations purchased commercially were not as stable as clinical formulations of PL, such as Doxil®. We thus only utilized PET/CT data from the first hour post-infusion in validating our PBPK model.

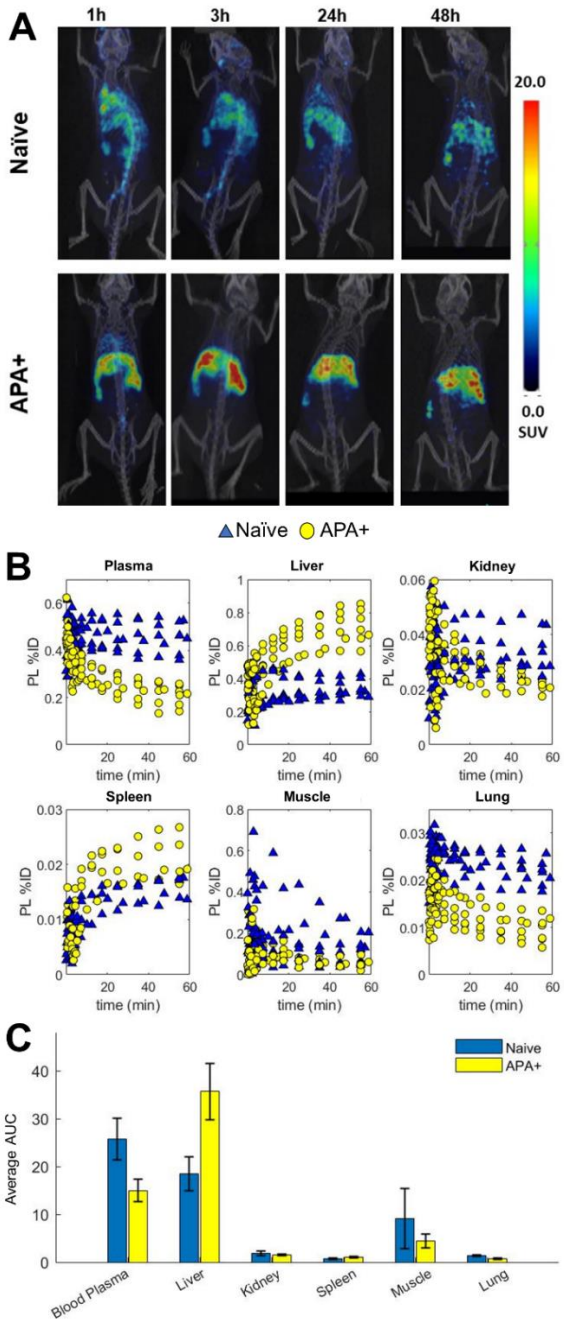

Figure 1.2. Comparison Between APA+ and Naïve Mice. (A) PET/CT imaging for a representative APA+ and naïve mouse. Note the substantial liver uptake within the first hour of study, particularly in the APA+ mouse. (B) Quantity of PL in the blood and different organs in APA-sensitized (n=6, yellow filled circle) vs. naïve (n=6, blue filled triangle) mice: (i) Blood, (ii) Liver, (iii) Kidney, (iv) Spleen, (v) Muscle, and (vi) Lung. (1 = 100 %ID). (C) Comparison of 1 h AUC of percent injected dose in each organ for APA-sensitized vs. naïve mice. Error bars represent standard deviation.

PBPK model accurately captures early phase APA-mediated clearance of PL

We first sought to confirm that our PBPK model can accurately reproduce the PK and biodistribution of PL in the absence of APA over the first hour, using parameter values that are reflective of the mouse anatomy and physiology. When calibrating our model parameters, we used a threshold of no more than 10% error for each organ (normalized to total signal in the mouse) to stop the optimization process; for most of the data, the error is less than 5%. With minimal optimization, our PBPK model accurately reproduced not only the correct concentration of PL in both plasma and the major organs of interest, but also the change in concentrations over time (Figure 1.3A, 1.4, 1.5). We noticed appreciably greater variations in the data from model predictions in the initial few minutes post-infusion (Figure 1.6), which is likely attributed to fluctuations in the initial PET signal immediately following infusion. We also noticed generally greater deviations between model prediction and PET/CT measurements of the muscle compartment, which is likely attributed to the low intensity of the signal in this organ resulting in a high signal-to-noise ratio (Figure 1.6).

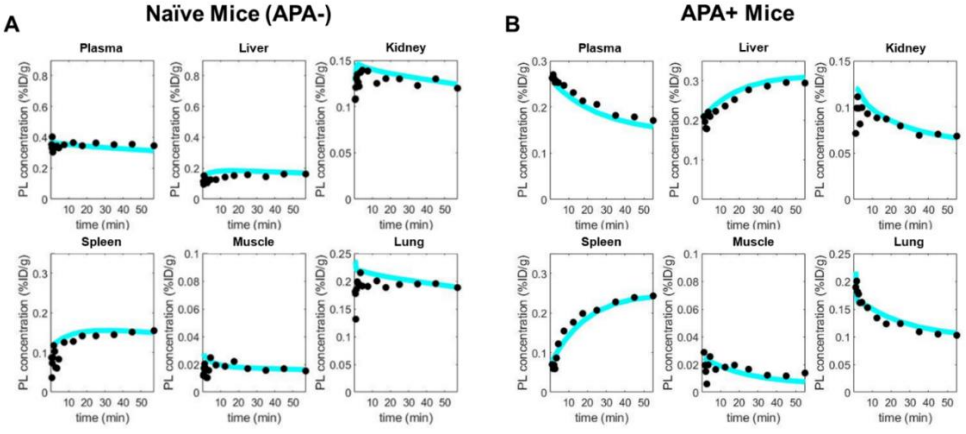

Figure 1.3. Comparison of PBPK Model Predictions. Comparison of PBPK model predictions vs. *in vivo* PET/CT imaging data for (A) a representative naïve mouse and (B) a representative APA+ mouse (37 µg/mL IgG), reported as %ID/g (1 = 100 %ID/g). Black closed circles represent measurements from PET/CT imaging, whereas turquoise line represents predictions from PBPK model.

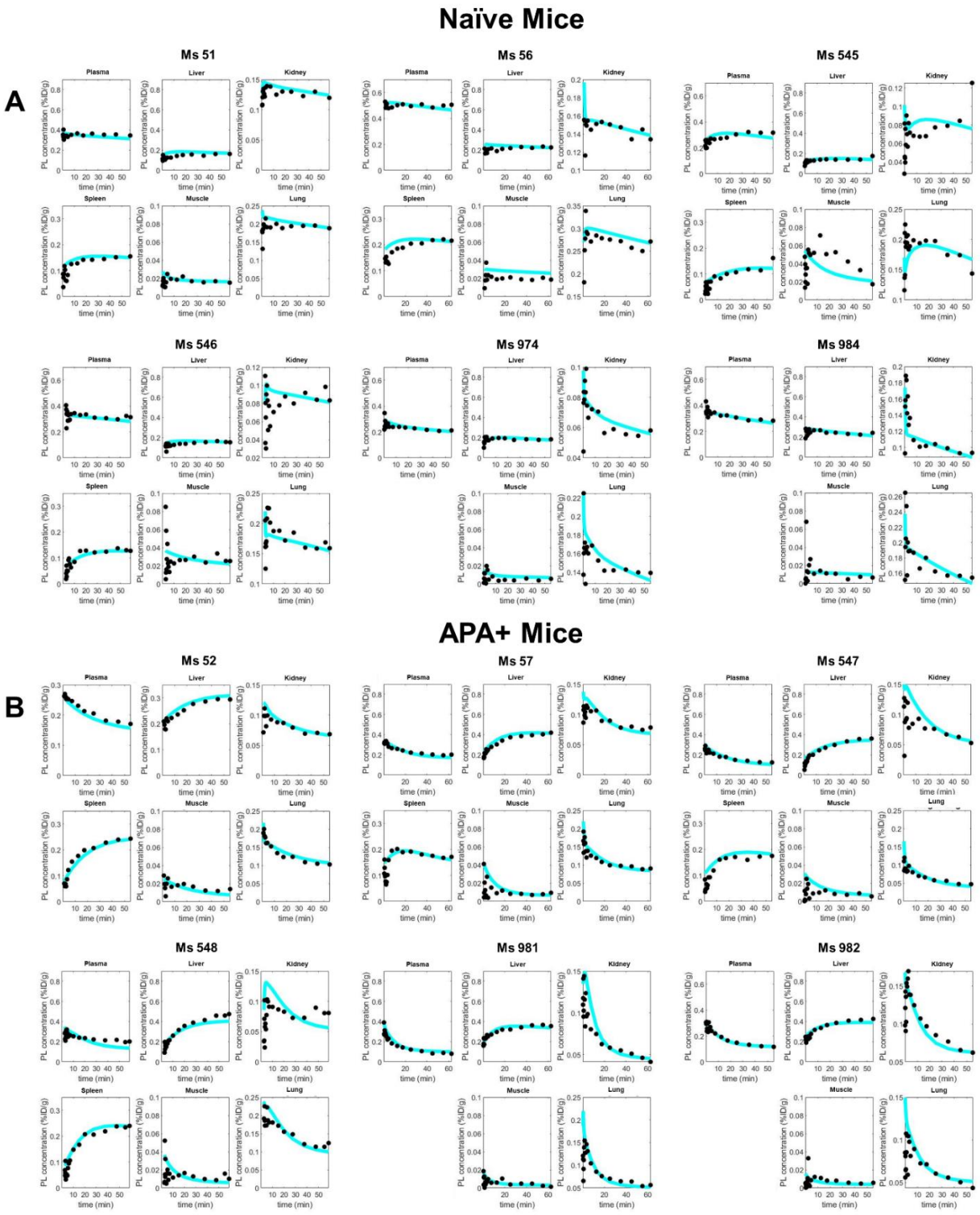

Figure 1.4. Example PBPK Model Fit. Example PBPK model fit in (A) naïve (n=6) and (B) APA+ (n=6) mice, illustrating that the model is able to accurately capture differences in physiology between mice as well as between cohorts (1 = 100 %ID/g). Spleen data is not available for 2 of the mice in each cohort.

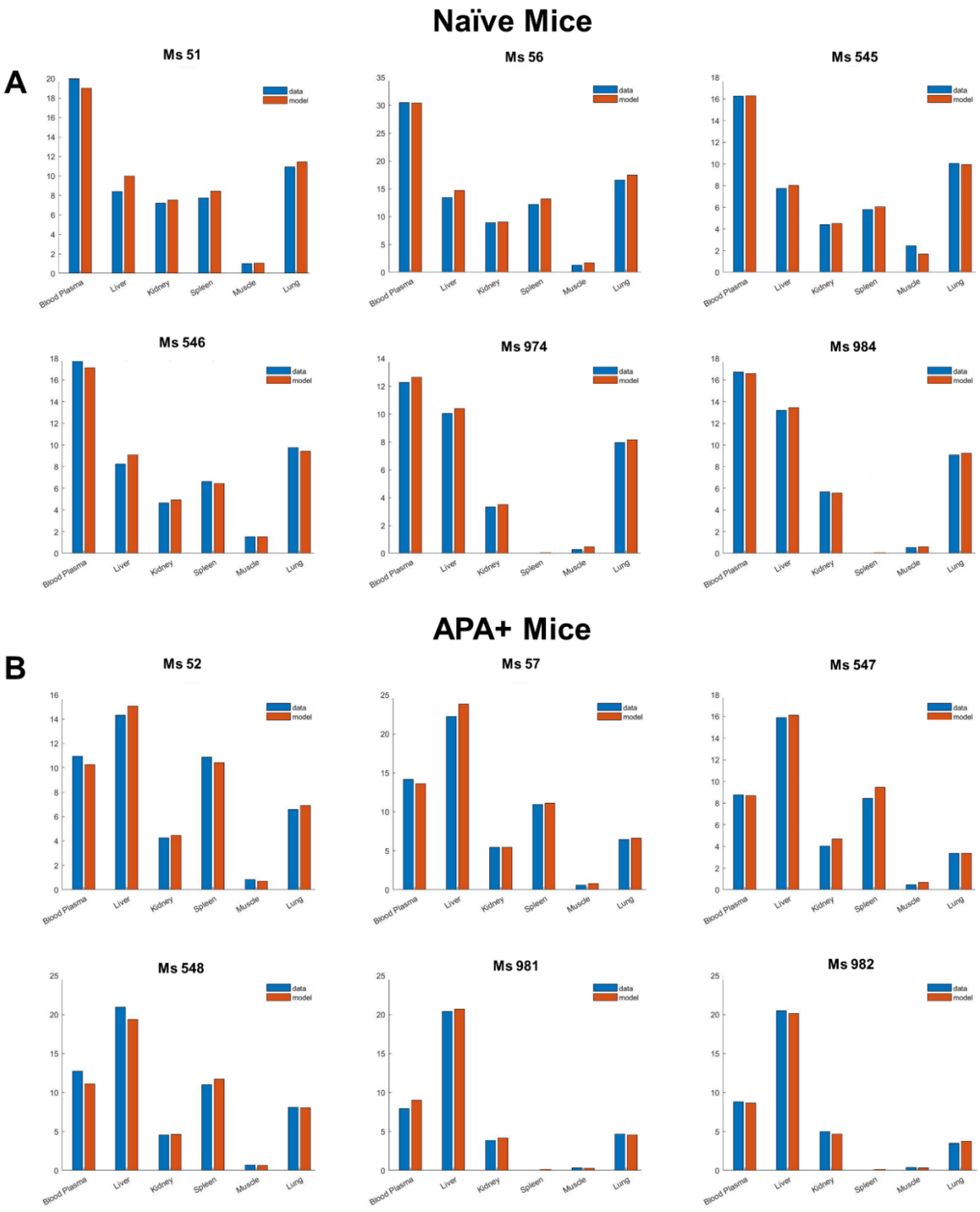

Figure 1.5. Example AUC from the PBPK Model Fit. Example AUC from the PBPK model fit in (A) naïve (n=6) and (B) APA+ (n=6) mice, illustrating that the model is able to accurately capture differences in physiology between mice as well as between cohorts. Spleen data is not available for 2 of the mice in each cohort.

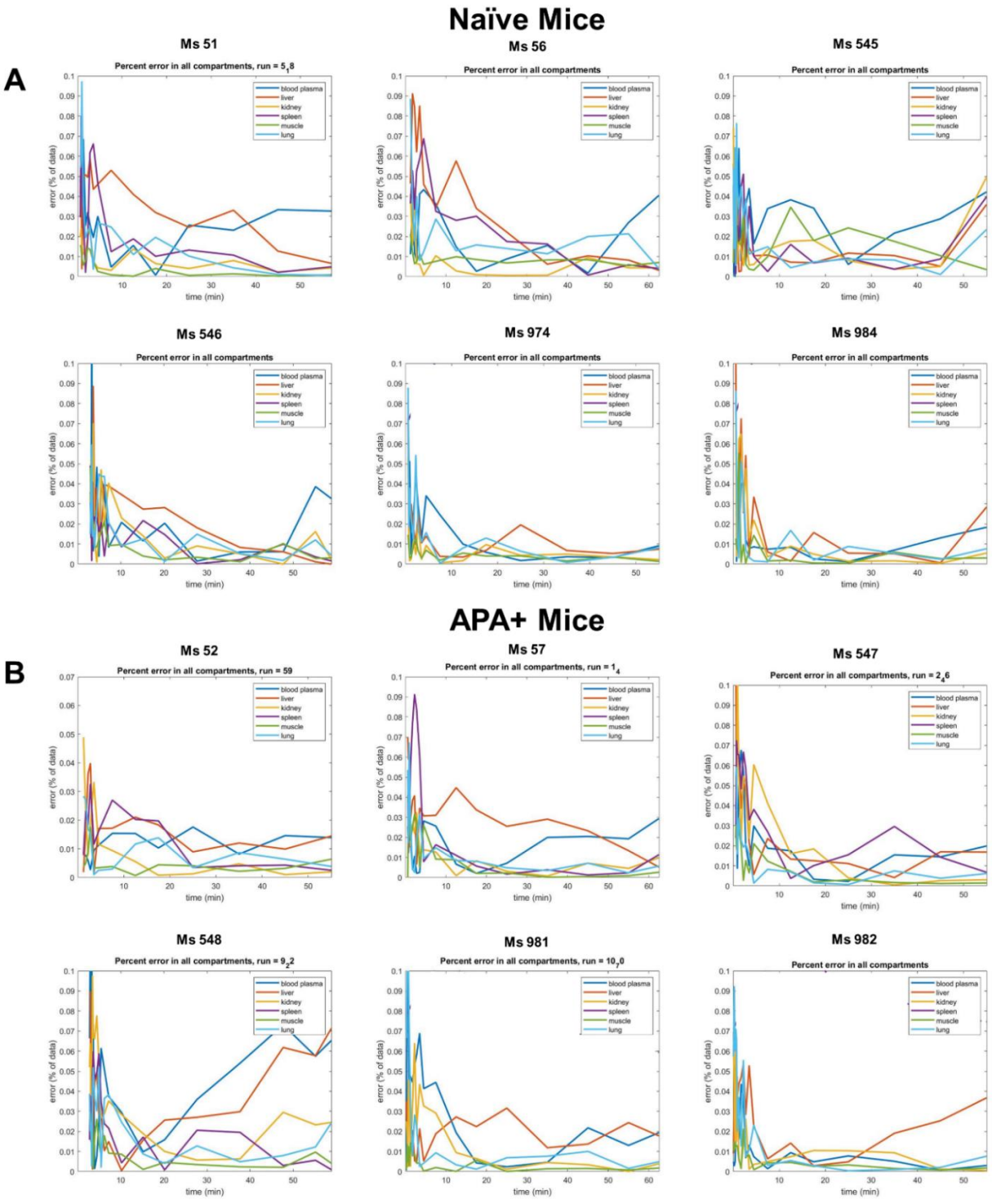

Figure 1.6. Example Error in the PBPK Model Prediction. Example error in the PBPK model fit in (A) naïve (n=6) and (B) APA+ (n=6) mice, illustrating that the model is able to accurately capture differences in physiology between mice as well as between cohorts (1 = 100%). Spleen data is not available for 2 of the mice in each cohort.

We next assessed the ability of our PBPK model to recapitulate APA-mediated clearance of PL from the blood to the liver and spleen. In our previous work on developing a minimal PBPK model for APA-mediated clearance of PL [40], we had already developed the algorithms to tally the rates of APA accumulation on PL over time as a function of APA titers. Thus, for the current more comprehensive PBPK model, once we validated our ability to model the fate of PL over time in the absence of APA, we simply needed to account for the affinity between APA/PL complexes and the accumulation potentials on key organs (captured in the *Kp* value for each organ). With these additions, our model was able to capture the initial transient dynamics of PL circulation and accumulation in different organs in mice with substantial APA titers (Figure 1.3B, 1.4-1.6). Not surprisingly, AUC predictions from the model closely matched experimental measurements (Figure 1.5, 1.7).

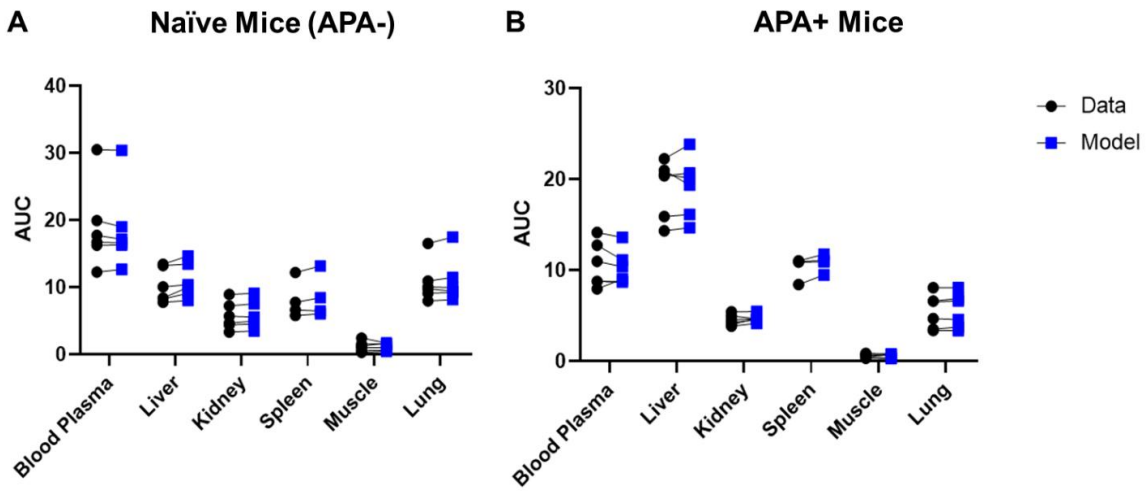

Figure 1.7. Model and Experimental Data AUC at 1h. AUC at 1h predicted by the PBPK model (black filled circle) vs. PET/CT data (blue filled square), for (A) naïve and (B) APA+ mice. AUC values were computed from %ID/g in each organ as a numerical integral in MATLAB.

PBPK models can make predictions that are often difficult to directly test *in vivo*. For instance, PET/CT imaging does not offer the resolution needed to differentiate the fraction of drug found in the blood vasculature within an organ vs. in the cells/tissue interstitium. Utilizing parameters that are largely consistent with other PBPK models (and thus reflective of the mouse physiology), our PBPK model predicts that a substantial fraction of PL begins to distribute to the liver within the first 5 minutes post infusion, initially within the blood vasculature. It is at this point that the time series curves tracking PL in plasma of naïve and APA+ mice began to diverge. In naïve mice, residual blood (in the liver) continued to account for most of the predicted signal in the liver. In contrast, in APA+ mice, the model predicts that within 15 minutes, a substantial fraction of PL can begin to extravasate from local blood vasculature into the cells and tissues, with the amount of PL in the cells and tissues in the liver dominant over the amount in the local plasma sub-compartment. Such preferential distribution of PL was necessary for the model to faithfully reproduce the observed plasma PK and biodistribution data in both naïve and PL-sensitized, APA+ mice. Indeed, while all of the APA+ mice had a distinct extravasation point in the liver compartment, none of the naïve mice exhibited this behavior. Consistent with physiological trends in the data, the rate of change in drug distribution to the lung and kidney compartments tended to mirror those in the plasma (which indicates no appreciable distribution to cells and tissues within those organs), whereas the concentrations in the spleen tended to mirror those in the liver, consistent with the abundance of cells with Fc receptors that can intercept and retain APA-immune complexes.

PBPK model also recapitulates APA-mediated clearance of PL over long timescales

Finally, our goal was to develop a comprehensive PBPK model that can recapitulate not only the early fate of PEGylated drug carriers but also their PK and biodistribution over longer timescales. To assess the predictive power of our model over the course of days, we tested our model against our prior data set, capturing the fate of Doxil® (PEGylated liposomal doxorubicin) in mice with and without APA [40]. The APA+ mice in this data set possessed anti-PEG IgG levels of ~0.3 μg/mL, enough to induce ABC of PL, but lower than the APA levels in PL-sensitized mice from our PET/CT studies. We had to fine-tune model parameters to account for the fact that Doxil® has a longer systemic persistence than the PL used in our PET/CT studies. Our model accurately recapitulated the PK and biodistribution of the drug in the liver, lung, and spleen over a 96-hour period (Figure 1.8), underscoring the model's ability to capture the fate of PL at both short and long timescales. It should be noted that minimal tuning of the other model parameters was necessary, and the only notable difference was lower splenic uptake of Doxil® at later time points. This suggests that the model accurately captures the physiology of APA-mediated accelerated clearance, and that it is generally adaptable to predicting PK of other drugs and assessment through alternate experimental designs.

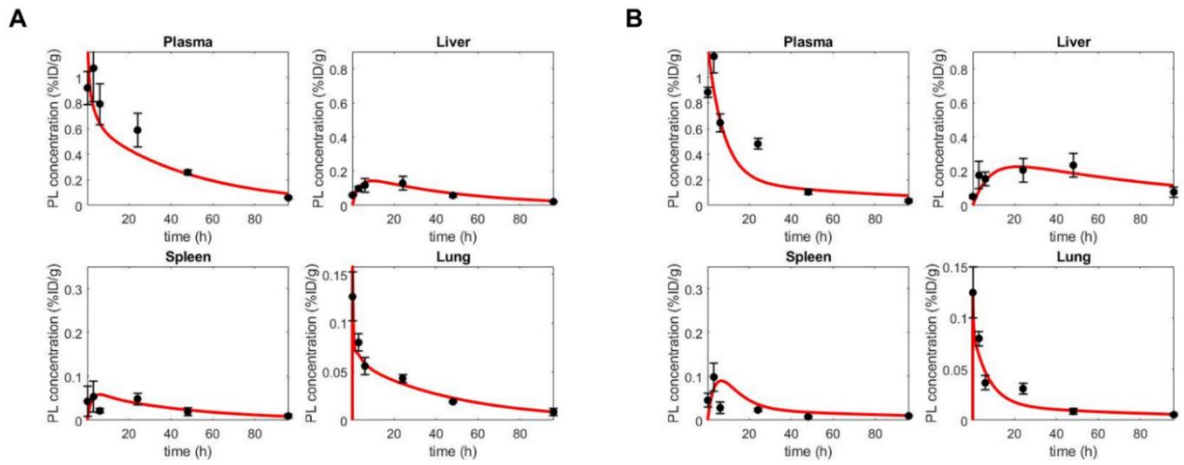

Figure 1.8. PBPK Model Recapitulates Historical Data. PBPK model recapitulates Doxil® pharmacokinetics and distribution in (A) naïve mice and (B) APA+ mice over 96h, reported in %ID/g (1 = 100 %ID/g). Black closed circles represent Doxil® levels measured by HPLC from Ref [40], whereas red line represents predictions from the current PBPK model. This data reflects the average Doxil® level from 3 mice sacrificed at each time point (5min, 3h, 6h, 24h, 48h, 96h).

Discussion

Numerous clinical trials have shown that our immune system can secrete APA – effectively a form of ADA – that in turn can directly reduce efficacy and/or trigger hypersensitivity reactions to at least select PEGylated therapeutics. A distinguishing feature of APA vs. classical ADA is that APA can be present prior to initial dosing of the therapeutics, and can also be elicited by other therapies containing PEG or PEG-conjugates. Furthermore, while clinical studies to date indicate only a small number of PEGylated drugs are impacted by APA, those clinical studies effectively reflect *only* the immunogenicity profiles of the PEGylated drugs being investigated, as the primary and secondary endpoints generally focus on the safety and efficacy of the drug following repeated dosing. Due to the nature of the study design, these clinical studies typically do not reflect the efficacy and safety of the PEGylated drugs when dosed into patients with high APA titers elicited by other means, for instance by other more

immunogenic PEGylated drugs. Given the increasing number of PEGylated drugs that are FDA-approved or in clinical development, including the unprecedented scale with which mRNA vaccines stabilized with PEG-lipid conjugates are deployed as a consequence of the COVID pandemic, we are likely entering a new era where the polypharmacy risks associated with APA are greater than ever before. In turn, this likely necessitates a new series of tools and approaches for addressing the APA polypharmacy issues.

PBPK models offer a powerful tool to understand, interpret and possibly intervene in risks presented by APA to patients, even in the absence of data from controlled clinical trials. Although a number of mathematical models have been published [49, 50], quantitative insights into the interactions between ADA and their therapeutic targets remain very limited. Indeed, it is difficult to experimentally tease apart complex binding interactions in living systems. The likely demand for more powerful predictive tools for APA motivated us to expand on our minimal PBPK model to develop a comprehensive PBPK model that can accurately recapitulate the circulation profiles of PEGylated drugs and liposomes in the presence of APA. While PBPK modeling is largely mechanistic, the combination of mechanistic and data-driven approaches in such models improves their accuracy and predictive ability [51-53]. Here, we validated our PBPK model against both PK and biodistribution data from PET/CT imaging as well as classical assessment of drug concentrations. Our PBPK model was able to accurately recapitulate the *in vivo* fate of PL at both short and long timescales. We believe our model not only can guide animal studies of PEG-immunogenicity, but also serves as a promising platform for interpreting the impact of APA in PEG-sensitized patients in clinical settings.

From both experimental studies and model predictions, it is abundantly clear that PL are rapidly cleared from the systemic circulation in APA+ mice, with liver representing the dominant

organ of distribution. In contrast, naïve mice exhibited substantially slower clearance, with PL levels in the spleen comparable to or above those in the liver. Assuming the vasculature and general tissue permeability that governs extravasation of PL should be the same between naïve and APA+ mice, our PBPK model indicates that the distinct PK and biodistribution of PL driven by APA must be attributed to interactions between cells possessing Fc receptors that can bind extravasated APA/PL immune-complexes. In other words, the primary driver of APA-mediated clearance of PL from the circulation is unlikely due to preferential distribution of PL from the circulation into a local plasma compartment, but rather enhanced retention of PL that has already been distributed to the liver. Not surprisingly, due to the abundance of cells possessing FcR in the liver, the liver is the dominant organ of APA clearance.

Some disparity between the predicted and observed blood plasma concentrations and clearance can be attributed to the use of PET data from the heart as a proxy for plasma. This data collection process may have captured a low level of additional heart tissue signal, which could not be determined at a high enough resolution to separate. The initial peaks of signal post-injection may not have been fully captured during PET imaging due to image resolution, saturation, and binning limitations. It is also acknowledged that free ^{64}Cu or ^{89}Zr isotope accumulation by the intracellular compartments could have contributed to some of the observed PET signals. There is also the possibility of minimal signal in organs not specifically accounted for, such as the brain, though this has been absorbed into the "remainder" compartment. However, Cu labeling is a common and accepted method for tracking biodistribution with consistent signals [54, 55].

In conclusion, we have demonstrated our ability to track the fate of PEGylated drug carriers while capturing some complexities of physiology that may significantly impact the

dynamics of APA-mediated clearance with high temporal resolution. Our model holds promise for answering questions about the dynamics of APA in the systemic circulation. More broadly, we expect our model to provide important mechanistic insights into monoclonal antibody-mediated clearance of pathogens as well as other ADA. With our PBPK model, we can explicitly track the binding dynamics of various species in the system, as a multiscale process, rather than as an average phenomenon related to how their effects are propagated. This model lays a framework for testing possible interventions to mitigate APA-mediated accelerated blood clearance. For example, we have previously shown that pre-injection with a high molecular weight free PEG (unbound to drug carriers) can increase the circulation time of PEGylated therapeutics even in the presence of APA [39]. When free PEG is injected into the bloodstream, the APA form complexes with and clear the PEG rather than the drug [39]. Future modeling efforts aim to incorporate the dynamics of free PEG interactions with APA and PEG-liposomes, with the goal of preventing APA-mediated clearance and thus enabling the safe and efficacious use of PEGylated therapeutics in individuals with APA.

Acknowledgments

Animal studies were performed within the UNC Lineberger Animal Studies Core at the University of North Carolina at Chapel Hill which is supported in part by an NCI Center Core Support Grant (CA16086) to the UNC Lineberger Comprehensive Cancer Center. The authors would like to thank BRIC Small Animal Imaging core facility for providing the PET/CT imaging service. The imaging core is supported in part by an NCI Grant P30-CA016086. The PET/CT system is supported by NIH instrumentation grant, S10-OD023611.

REFERENCES

[1] K. Knop, R. Hoogenboom, D. Fischer, U.S. Schubert, Poly(ethylene glycol) in Drug Delivery: Pros and Cons as Well as Potential Alternatives, Angewandte Chemie International Edition, 49 (2010) 6288-6308.

[2] I.A. Ivens, W. Achanzar, A. Baumann, A. Brändli-Baiocco, J. Cavagnaro, M. Dempster, B.O. Depelchin, A.R. Irizarry Rovira, L. Dill-Morton, J.H. Lane, B.M. Reipert, T. Salcedo, B. Schweighardt, L.S. Tsuruda, P.L. Turecek, J. Sims, PEGylated Biopharmaceuticals: Current Experience and Considerations for Nonclinical Development, Toxicologic pathology, 43 (2015) 959-983.

[3] M. Swierczewska, K.C. Lee, S. Lee, What is the future of PEGylated therapies?, Expert opinion on emerging drugs, 20 (2015) 531-536.

[4] T. Gefen, J. Vaya, S. Khatib, N. Harkevich, F. Artoul, E.D. Heller, J. Pitcovski, E. Aizenshtein, The impact of PEGylation on protein immunogenicity, International immunopharmacology, 15 (2013) 254-259.

[5] F.M. Veronese, A. Mero, The impact of PEGylation on biological therapies, BioDrugs : clinical immunotherapeutics, biopharmaceuticals and gene therapy, 22 (2008) 315-329.

[6] F.M. Veronese, G. Pasut, PEGylation, successful approach to drug delivery, Drug discovery today, 10 (2005) 1451-1458.

[7] S. Jevsevar, M. Kunstelj, V.G. Porekar, PEGylation of therapeutic proteins, Biotechnology journal, 5 (2010) 113-128.

[8] Q. Yang, S.K. Lai, Anti-PEG immunity: emergence, characteristics, and unaddressed questions, Wiley interdisciplinary reviews. Nanomedicine and nanobiotechnology, 7 (2015) 655-677.

[9] X. Wan, J. Zhang, W. Yu, L. Shen, S. Ji, T. Hu, Effect of protein immunogenicity and PEG size and branching on the anti-PEG immune response to PEGylated proteins, Process Biochemistry, 52 (2017) 183-191.

[10] B. Li, Z. Yuan, H.-C. Hung, J. Ma, P. Jain, C. Tsao, J. Xie, P. Zhang, X. Lin, K. Wu, S. Jiang, Revealing the Immunogenic Risk of Polymers, Angewandte Chemie International Edition, 57 (2018) 13873-13876.

[11] Q. Yang, T.M. Jacobs, J.D. McCallen, D.T. Moore, J.T. Huckaby, J.N. Edelstein, S.K. Lai, Analysis of Pre-existing IgG and IgM Antibodies against Polyethylene Glycol (PEG) in the General Population, Analytical Chemistry, 88 (2016) 11804-11812.

[12] J.K. Armstrong, G. Hempel, S. Koling, L.S. Chan, T. Fisher, H.J. Meiselman, G. Garratty, Antibody against poly(ethylene glycol) adversely affects PEG-asparaginase therapy in acute lymphoblastic leukemia patients, Cancer, 110 (2007) 103-111.

[13] M.S. Hershfield, N.J. Ganson, S.J. Kelly, E.L. Scarlett, D.A. Jaggers, J.S. Sundy, Induced and pre-existing anti-polyethylene glycol antibody in a trial of every 3-week dosing of pegloticase for refractory gout, including in organ transplant recipients, Arthritis Research & Therapy, 16 (2014) R63.

[14] P.E. Lipsky, L.H. Calabrese, A. Kavanaugh, J.S. Sundy, D. Wright, M. Wolfson, M.A. Becker, Pegloticase immunogenicity: the relationship between efficacy and antibody development in patients treated for refractory chronic gout, Arthritis Research & Therapy, 16 (2014) R60.

[15] J.S. Sundy, N.J. Ganson, S.J. Kelly, E.L. Scarlett, C.D. Rehrig, W. Huang, M.S. Hershfield, Pharmacokinetics and pharmacodynamics of intravenous PEGylated recombinant mammalian urate oxidase in patients with refractory gout, Arthritis & Rheumatism, 56 (2007) 1021-1028.

[16] N. Longo, C.O. Harding, B.K. Burton, D.K. Grange, J. Vockley, M. Wasserstein, G.M. Rice, A. Dorenbaum, J.K. Neuenburg, D.G. Musson, Z. Gu, S. Sile, Single-dose, subcutaneous recombinant phenylalanine ammonia lyase conjugated with polyethylene glycol in adult patients with phenylketonuria: an open-label, multicentre, phase 1 dose-escalation trial, Lancet (London, England), 384 (2014) 37-44.

[17] A.S. Abu Lila, H. Kiwada, T. Ishida, The accelerated blood clearance (ABC) phenomenon: Clinical challenge and approaches to manage, Journal of Controlled Release, 172 (2013) 38-47.

[18] S.M. Fix, A.G. Nyankima, M.D. McSweeney, J.K. Tsuruta, S.K. Lai, P.A. Dayton, Accelerated Clearance of Ultrasound Contrast Agents Containing Polyethylene Glycol is Associated with the Generation of Anti-Polyethylene Glycol Antibodies, Ultrasound in Medicine & Biology, 44 (2018) 1266-1280.

[19] M. Ichihara, T. Shimizu, A. Imoto, Y. Hashiguchi, Y. Uehara, T. Ishida, H. Kiwada, Anti-PEG IgM Response against PEGylated Liposomes in Mice and Rats, Pharmaceutics, 3 (2010) 1-11.

[20] T. Ishida, M. Harada, X.Y. Wang, M. Ichihara, K. Irimura, H. Kiwada, Accelerated blood clearance of PEGylated liposomes following preceding liposome injection: Effects of lipid dose and PEG surface-density and chain length of the first-dose liposomes, Journal of Controlled Release, 105 (2005) 305-317.

[21] T. Ishida, X. Wang, T. Shimizu, K. Nawata, H. Kiwada, PEGylated liposomes elicit an anti-PEG IgM response in a T cell-independent manner, Journal of Controlled Release, 122 (2007) 349-355.

[22] M. Mohamed, A.S. Abu Lila, T. Shimizu, E. Alaaeldin, A. Hussein, H.A. Sarhan, J. Szebeni, T. Ishida, PEGylated liposomes: immunological responses, Science and Technology of Advanced Materials, 20 (2019) 710-724.

[23] T.C. Chang, B.M. Chen, W.W. Lin, P.H. Yu, Y.W. Chiu, Y.T. Chen, J.Y. Wu, T.L. Cheng, D.Y. Hwang, A.S. Roffler, Both IgM and IgG Antibodies Against Polyethylene Glycol Can

Alter the Biological Activity of Methoxy Polyethylene Glycol-Epoetin Beta in Mice, Pharmaceutics, 12 (2019).

[24] L.P. Ganesan, Y. Kim J Fau - Wu, S. Wu Y Fau - Mohanty, G.S. Mohanty S Fau - Phillips, D.J. Phillips Gs Fau - Birmingham, J.M. Birmingham Dj Fau - Robinson, C.L. Robinson Jm Fau - Anderson, C.L. Anderson, FcγRIIb on liver sinusoidal endothelium clears small immune complexes.

[25] G.T. Kozma, T. Shimizu, T. Ishida, J. Szebeni, Anti-PEG antibodies: Properties, formation, testing and role in adverse immune reactions to PEGylated nano-biopharmaceuticals, Advanced Drug Delivery Reviews, (2020).

[26] G.T. Kozma, T. Mészáros, I. Vashegyi, T. Fülöp, E. Örfi, L. Dézsi, L. Rosivall, Y. Bavli, R. Urbanics, T.E. Mollnes, Y. Barenholz, J. Szebeni, Pseudo-anaphylaxis to Polyethylene Glycol (PEG)-Coated Liposomes: Roles of Anti-PEG IgM and Complement Activation in a Porcine Model of Human Infusion Reactions, ACS Nano, 13 (2019) 9315-9324.

[27] L.H. Calabrese, A. Kavanaugh, A.E. Yeo, P.E. Lipsky, Frequency, distribution and immunologic nature of infusion reactions in subjects receiving pegloticase for chronic refractory gout, Arthritis Research & Therapy, 19 (2017) 191.

[28] J.S. Sundy, H.S.B. Baraf, R.A. Yood, N.L. Edwards, S.R. Gutierrez-Urena, E.L. Treadwell, J. Vázquez-Mellado, W.B. White, P.E. Lipsky, Z. Horowitz, W. Huang, A.N. Maroli, R.W. Waltrip, II, S.A. Hamburger, M.A. Becker, Efficacy and Tolerability of Pegloticase for the Treatment of Chronic Gout in Patients Refractory to Conventional Treatment: Two Randomized Controlled Trials, JAMA, 306 (2011) 711-720.

[29] T.J. Povsic, M.G. Lawrence, A.M. Lincoff, R. Mehran, C.P. Rusconi, S.L. Zelenkofske, Z. Huang, J. Sailstad, P.W. Armstrong, P.G. Steg, C. Bode, R.C. Becker, J.H. Alexander, N.F. Adkinson, A.I. Levinson, Pre-existing anti-PEG antibodies are associated with severe immediate allergic reactions to pegnivacogin, a PEGylated aptamer, Journal of Allergy and Clinical Immunology, 138 (2016) 1712-1715.

[30] F. Cox, K. Khalib, N. Conlon, PEG That Reaction: A Case Series of Allergy to Polyethylene Glycol, The Journal of Clinical Pharmacology, n/a (2021).

[31] J. Kleine-Tebbe, L. Klimek, E. Hamelmann, O. Pfaar, C. Taube, M. Wagenmann, T. Werfel, M. Worm, Severe allergic reactions to the COVID-19 vaccine - statement and practical consequences, Allergol Select, 5 (2021) 26-28.

[32] M. Worm, A. Bauer, B. Wedi, R. Treudler, W. Pfuetzner, K. Brockow, T. Buhl, T. Zuberbier, J. Fluhr, G. Wurpts, L. Klimek, T. Jacob, H.F. Merk, N. Mülleneisen, S. Roeseler, H. Dickel, U. Raap, J. Kleine-Tebbe, Practical recommendations for the allergological risk assessment of the COVID-19 vaccination - a harmonized statement of allergy centers in Germany, Allergol Select, 5 (2021) 72-76.

[33] C. Walsh, J.J. Bonner, T.N. Johnson, S. Neuhoff, E.A. Ghazaly, J.G. Gribben, A.V. Boddy, G.J. Veal, Development of a physiologically based pharmacokinetic model of actinomycin D in children with cancer, British journal of clinical pharmacology, 81 (2016) 989-998.

[34] E. Rouits, P. Guichard S Fau - Canal, E. Canal P Fau - Chatelut, E. Chatelut, Non-linear pharmacokinetics of irinotecan in mice.

[35] W. Zhou, T.N. Johnson, H. Xu, S. Cheung, K.H. Bui, J. Li, N. Al-Huniti, D. Zhou, Predictive Performance of Physiologically Based Pharmacokinetic and Population Pharmacokinetic Modeling of Renally Cleared Drugs in Children, CPT Pharmacometrics Syst Pharmacol, 5 (2016) 475-483.

[36] H.-T. Thai, F. Mazuir, S. Cartot-Cotton, C. Veyrat-Follet, Optimizing pharmacokinetic bridging studies in paediatric oncology using physiologically-based pharmacokinetic modelling: application to docetaxel, British journal of clinical pharmacology, 80 (2015) 534-547.

[37] M.J. Eigenmann, T.V. Karlsen, B.-F. Krippendorff, O. Tenstad, L. Fronton, M.B. Otteneder, H. Wiig, Interstitial IgG antibody pharmacokinetics assessed by combined in vivo- and physiologically-based pharmacokinetic modelling approaches, J Physiol, 595 (2017) 7311-7330.

[38] A. Garg, J.P. Balthasar, Physiologically-based pharmacokinetic (PBPK) model to predict IgG tissue kinetics in wild-type and FcRn-knockout mice, Journal of Pharmacokinetics and Pharmacodynamics, 34 (2007) 687-709.

[39] M.D. McSweeney, L.S.L. Price, T. Wessler, E.C. Ciociola, L.B. Herity, J.A. Piscitelli, A.C. DeWalle, T.N. Harris, A.K.P. Chan, R.S. Saw, P. Hu, J.C. Jennette, M.G. Forest, Y. Cao, S.A. Montgomery, W.C. Zamboni, S.K. Lai, Overcoming anti-PEG antibody mediated accelerated blood clearance of PEGylated liposomes by pre-infusion with high molecular weight free PEG, Journal of Controlled Release, 311-312 (2019) 138-146.

[40] M.D. McSweeney, T. Wessler, L.S.L. Price, E.C. Ciociola, L.B. Herity, J.A. Piscitelli, W.C. Zamboni, M.G. Forest, Y. Cao, S.K. Lai, A minimal physiologically based pharmacokinetic model that predicts anti-PEG IgG-mediated clearance of PEGylated drugs in human and mouse, Journal of Controlled Release, 284 (2018) 171-178.

[41] M.D. McSweeney, L. Shen, A.C. DeWalle, J.B. Joiner, E.C. Ciociola, D. Raghuwanshi, M.S. Macauley, S.K. Lai, Pre-treatment with high molecular weight free PEG effectively suppresses anti-PEG antibody induction by PEG-liposomes in mice, Journal of Controlled Release, (2020).

[42] M.J.W.D. Vosjan, L.R. Perk, G.W.M. Visser, M. Budde, P. Jurek, G.E. Kiefer, G.A.M.S. van Dongen, Conjugation and radiolabeling of monoclonal antibodies with zirconium-89 for PET imaging using the bifunctional chelate p-isothiocyanatobenzyl-desferrioxamine, Nature Protocols, 5 (2010) 739-743.

[43] B. Davies, T. Morris, Physiological Parameters in Laboratory Animals and Humans, Pharmaceutical Research, 10 (1993) 1093-1095.

[44] R.P. Brown, S.L. Delp Md Fau - Lindstedt, L.R. Lindstedt Sl Fau - Rhomberg, R.P. Rhomberg Lr Fau - Beliles, R.P. Beliles, Physiological parameter values for physiologically based pharmacokinetic models.

[45] N. Kaliss, D. Pressman, Plasma and blood volumes of mouse organs, as determined with radioactive iodoproteins, Proceedings of the Society for Experimental Biology and Medicine. Society for Experimental Biology and Medicine (New York, N.Y.), 75 (1950) 16-20.

[46] H. Jones, K. Rowland-Yeo, Basic concepts in physiologically based pharmacokinetic modeling in drug discovery and development, CPT: pharmacometrics & systems pharmacology, 2 (2013) e63-e63.

[47] S. Marino, I.B. Hogue, C.J. Ray, D.E. Kirschner, A methodology for performing global uncertainty and sensitivity analysis in systems biology, Journal of Theoretical Biology, 254 (2008) 178-196.

[48] S.C. Hora, R.L. Iman, Expert Opinion in Risk Analysis: The NUREG-1150 Methodology, Nuclear Science and Engineering, 102 (1989) 323-331.

[49] X. Chen, T. Hickling, E. Kraynov, B. Kuang, C. Parng, P. Vicini, A mathematical model of the effect of immunogenicity on therapeutic protein pharmacokinetics, The AAPS journal, 15 (2013) 1141-1154.

[50] J.D. Gómez-Mantilla, I.F. Trocóniz, Z. Parra-Guillén, M.J. Garrido, Review on modeling anti-antibody responses to monoclonal antibodies, Journal of Pharmacokinetics and Pharmacodynamics, 41 (2014) 523-536.

[51] A.N. Edginton, E.I. Zimmerman, A. Vasilyeva, S.D. Baker, J.C. Panetta, Sorafenib metabolism, transport, and enterohepatic recycling: physiologically based modeling and simulation in mice, Cancer Chemotherapy and Pharmacology, 77 (2016) 1039-1052.

[52] M. Krauss, R. Burghaus, J. Lippert, M. Niemi, P. Neuvonen, A. Schuppert, S. Willmann, L. Kuepfer, L. Görlitz, Using Bayesian-PBPK modeling for assessment of inter-individual variability and subgroup stratification, In Silico Pharmacol, 1 (2013) 6-6.

[53] N. Tsamandouras, A. Rostami-Hodjegan, L. Aarons, Combining the ‘bottom up’ and ‘top down’ approaches in pharmacokinetic modelling: fitting PBPK models to observed clinical data, British Journal of Clinical Pharmacology, 79 (2015) 48-55.

[54] M. Cooper, R. Paul, K. Shaw, P. Blower, Which bifunctional chelator for immunoPET with Cu-64?, Journal of Nuclear Medicine, 52 (2011) 407.

[55] C. Cui, F. Wang, M.-R. Zhang, M. Hanyu, A. Hatori, J. Yui, G. Shao, Z. Yiding, Z. Wang, Synthesis, Biodistribution and Metabolic Analysis of Cu-64 Labeled PSMA-targeted Ligand, Journal of Nuclear Medicine, 57 (2016) 1385.

CHAPTER 2: EXPERIMENTAL DATA AND PBPK MODELING QUANTIFY ANTIBODY INTERFERENCE IN PEGYLATED DRUG CARRIER DELIVERY[2]

Summary

Physiologically-based pharmacokinetic (PBPK) mathematical modeling is a popular drug development tool that integrates physiology, drug physicochemical properties, preclinical data, and clinical information to predict drug systemic disposition. Since PBPK models seek to capture complex physiology, parameter uncertainty and variability is a prevailing challenge: there are often more compartments (e.g., organs, each with mechanisms for drug flux and retention, and their associated model parameters) than can be simultaneously measured. To improve the fidelity of PBPK modeling, one approach is to search and optimize within the high-dimensional model parameter space, based on experimental time-series measurements of drug distributions in a subset of the compartments. Here, we employ Latin Hypercube Sampling (LHS) on a PBPK model of PEGylated nanomedicines that tracks biodistribution in an 8-compartment mouse circulatory system, in the presence (APA+) or absence (naïve) of anti-PEG antibodies (APA). Near-continuous experimental measurements of drug concentration during the first hour post drug injection from the liver, spleen, kidney, muscle, lung, and blood plasma are used as truth sets with LHS to infer optimal parameter ranges for the full PBPK model, for both APA+ and naïve mice. The data and model quantify that drug retention in the liver is the primary (and spleen the secondary) differentiator of the biodistribution patterns of PL in naïve versus APA+

[2] This chapter is adapted from a preprint of an article submitted to the Bulletin of Mathematical Biology. The original citation is as follows:
Talkington A.M., Wessler T., Lai S.K., Cao Y., Forest M.G. "Experimental data and PBPK modeling quantify antibody interference in PEGylated drug carrier delivery," Bulletin of Mathematical Biology (submitted).

mice, with retention of PEGylated nanomedicines substantially amplified in APA+ mice, due to PL-bound APA binding to receptors in the liver and spleen. We thereby reveal a mechanistic understanding of the biodistribution and APA-mediated clearance of PEGylated drugs.

Introduction

Drug development generally involves extensive studies in animal models to assess the pharmacokinetics and biodistribution of the drug over time, as the complex interactions between the drug and different elements of a living system cannot be readily captured by *in vitro* experiments. To interpret and guide animal studies, physiologically-based pharmacokinetic (PBPK) models are increasingly used to integrate drug and system (physiology) information into a mathematical modeling framework to describe and predict the absorption, distribution, metabolism and excretion of the drug in humans and animals. A key feature of PBPK models is their mechanistic focus, capturing the mass balance of the drug of interest over time by incorporating the anatomical, physiological, physical, and chemical processes that govern the eventual distribution of a drug. Many PBPK parameters are pre-determined experimentally – for example, organ-specific blood flow rates and volumes have been determined using appropriate radioactive tracers for a variety of model organisms [1-4]. PBPK models, coupled with the principle of allometric scaling, enable ease in translations across species and populations [5-7]. Not surprisingly, PBPK models are broadly adopted in drug development and regulation [8, 9], including the prediction of drug-drug interactions [10, 11], dose adjustment in special populations [12, 13], bioequivalence assessment of complex drug formulations [14, 15], and many other mechanistic explorations [16-20].

A limiting aspect of PBPK models is that some, and often many, key parameters are not well-documented. This is especially true in the development of new therapeutics. The complexity of living systems, as reflected by a large number of model parameters together with ethical as well as practical limitations, makes it difficult to measure or estimate all parameter values. This necessitates the use of various mathematical and statistical techniques to identify the most sensitive model parameters, and to take measures to better estimate those parameters in order to improve the predictive power of the PBPK model. Examples include variable response to treatment and individual-to-individual variability [21-23].

We previously developed a minimal, 2-compartment PBPK model to capture the systemic circulation over time of liposomal drug carriers modified with polyethylene glycol (PEG), or PEGylated liposomes (PL), in the presence of anti-PEG antibodies (APA) [24]. Clinically, APA have been shown to bind a number of PEGylated drugs. Above a critical threshold, APA cause rapid elimination of the PEGylated drugs from the circulation, greatly reducing their efficacy as well as increasing the adverse events associated with the therapy [25, 26]. Here, we expanded the minimal model to 8 compartments in order to better resolve the biodistribution of PEG-liposomes in the presence of APA. We compared the 8-component PBPK model predictions to experimental data obtained from tracing radiolabeled PL in different organ tissues over time, using positron emission tomography/computed tomography (PET/CT) scanning. Using the experimental measurements as truth sets, we then employed Latin Hypercube Sampling to deduce parameter ranges for the 8-compartment PBPK model for both APA+ and naïve mice. We identified principal parameters that induce the largest model variability, and used those principal components to optimize fits to the truth set with parameter range estimates. In doing so, we confirmed hypotheses for organs (liver and spleen) most

responsible for accelerated blood clearance (ABC) of PEGylated liposomes by anti-PEG antibodies. Further, we identified the specific kinetic mechanism (drug retention) amplified by the presence of APA as the driving factor for increased liver and spleen deposition.

Model Parametrization and Exploration

Parametrizing the Model with Latin Hypercube Sampling and Experimental Data

Here we introduce a full, multi-compartment PBPK model to describe the biodistribution of PL, and how it is altered in the presence of APA. The model was able to fit mouse data with and without APA, illustrating its capacity to recapitulate the accelerated blood clearance phenomenon mediated by APA. All of the mice in this study exhibited high APA titers (>15 µg/ml anti-PEG IgG), well above the threshold for ABC. The model accounts for the redistribution of radiolabeled PL from an IV injection through the lungs, liver, spleen, kidney, and muscle. A remainder compartment comprises the brain, adipose and other tissues that may sequester small amounts of the drug. Initializing the model at t = 1 min allows us to model the complete redistribution of drug to the appropriate organs, with some degree of noise, while eliminating excessive fluctuations due to very fast transient changes immediately post injection and limitations in the timing of the PET/CT imaging used to obtain the experimental data (i.e., a peak in signal that may appear and disappear between the 10-second windows used for binning images).

We consider the PBPK system defined by the following system of rate equations for transport of the "Drug" (PL) between all compartments (p = venous plasma, li = liver, k = kidney, s = spleen, m = muscle, a = arterial plasma, lu = lung, r = remainder compartment):

$$\frac{dC_p}{dt} = 1/V_p \cdot \left(-C_p \cdot CL_p\right) - Q_{lu} \cdot fr_{lu} \cdot C_p /V_p + (Q_{li} \cdot fr_{li} + Q_s \cdot fr_s)/V_p \cdot \left(C_{li} /Kp_{li}\right) + Q_m \cdot fr_m/V_p \cdot \left(C_m/Kp_m\right) + Q_k \cdot fr_k/V_p \cdot \left(C_k /Kp_k\right) + Q_r \cdot fr_r/V_p \cdot \left(C_r /Kp_r\right) \quad (1)$$

$$\frac{dC_{li}}{dt} = 1/V_{li} \cdot \left(Q_{li} \cdot fr_{li} \cdot C_a - (Q_{li} \cdot fr_{li} + Q_s \cdot fr_s) \cdot C_{li} ./Kp_{li}\right) + Q_s \cdot fr_s/V_{li} \cdot \left(C_s /Kp_s\right) - C_{li} /(Kp_{li} \cdot V_{li}) \cdot CL_{li} \quad (2)$$

$$\frac{dC_k}{dt} = Q_k \cdot fr_k/V_k \cdot \left(C_a - C_k /Kp_k\right) - C_k /(Kp_k \cdot V_k) \cdot CL_k \quad (3)$$

$$\frac{dC_s}{dt} = Q_s \cdot fr_s/V_s \cdot \left(C_a - C_s /Kp_s\right) \quad (4)$$

$$\frac{dC_m}{dt} = Q_m \cdot fr_m/V_m \cdot \left(C_a - C_m/Kp_m\right) \quad (5)$$

$$\frac{dC_a}{dt} = Q_{lu} \cdot fr_{lu}/V_a \cdot \left(C_{lu}/Kp_{lu}\right) - C_a \cdot (Q_{li} \cdot fr_{li}/V_a + Q_m \cdot fr_m/V_a + Q_s \cdot fr_s/V_a + Q_k \cdot fr_k/V_a + Q_r \cdot fr_r/V_a) \quad (6)$$

$$\frac{dC_{lu}}{dt} = Q_{lu} \cdot fr_{lu} \cdot C_p /V_{lu} - Q_{lu} \cdot fr_{lu} \cdot C_{lu}/(V_{lu} \cdot Kp_{lu}) \quad (7)$$

$$\frac{dC_r}{dt} = Q_r \cdot fr_r/V_r \cdot \left(C_a - C_r /Kp_r\right) \quad (8)$$

Here Q_x represents blood flow in compartment *x*, V_x represents the volume of tissue and interstitial components, C_x represents the concentration of PL (in %ID/g), CL_x represents clearance rate, fr_x represents the dimensionless permeability fraction controlling the extravasation rate into compartment *x*, and Kp_x represents the partitioning (drug retention) coefficient and the potential for accumulation in compartment *x*. A model incorporating permeability-limited distribution was chosen because the PL are ~100 nm in diameter, a sufficiently large size to make its extravasation rate much lower than blood perfusion.

In order to explore ranges for all parameters, we used Latin Hypercube Sampling (LHS). Rather than running parameter sweeps across the product space of ranges for all parameters, which is computationally impractical, LHS semi-randomly samples the product space of parameter ranges [27, 28]. We parametrized the system at the individual mouse level in order to consider inter-mouse and inter-cohort variability [29-31], and progressively refined parameter ranges based on LHS outputs for each *in silico* mouse.

To set limits of minimum and maximum possible parameter values, we first searched the literature. Some physiological parameters are well-documented in the literature, for example, blood flow and organ volume [1-4]. Further details such as residual blood volume allow us to determine an even more accurate approximation of the signal or drug concentration in each compartment [1, 4]. We selected a suitable initial range for the drug retention coefficients (Kp_x) per compartment from data, as the nearly continuous PET scan provided sufficient data to estimate Kp_x for each compartment as a function of its area under the curve (AUC). AUC for an organ compartment is computed as the integral of drug concentration over the duration of the study and is used as a measure of the organ's total drug exposure for this duration. Restrictions on values of these more well-documented parameters allowed us to perform a targeted exploration of less-known parameters, e.g., the organ permeability fraction (fr_x).

For the parameter ranges with less certainty, tests were used to determine parameter bounds that result in valid vs. invalid output. These pass/fail tests progressively narrow the parameter ranges in order to more reliably produce acceptable outputs. For the first round of tests, a parameter set was considered successful (passed) if (1) the model drug concentration in each organ was within 5-fold of *in vivo* experimental concentrations, (2) the AUC was within 20% of the AUC calculated from *in vivo* data, and (3) the remainder compartment was non-

negative and thus preserved mass balance. After completing a round of LHS simulations using relatively wide ranges for the least well-known parameters, each parameter range was examined to see which values yielded simulations that passed all tests and which values yielded simulations that failed at least one test. We found a representative parameter set whose model concentration and AUC plots visually resembled the *in vivo* experimental data and whose parameter values were not relatively close to values found in a failed test. From this representative parameter set, we created an updated range for each parameter by extending 10% above and below its value. Using these updated parameter ranges, we performed a second round of LHS simulations (Figure 2.1, 2.2). We sorted the model outputs (predicted drug concentration in each organ for the duration of the study) by the total sum of squared errors compared to the *in vivo* experimental data, and a characteristic parameter set for each mouse was selected from the ten with the lowest least-squares error. The least-squares error function was defined such that greater weight was placed on compartments with greater drug uptake, because errors were normalized by total signal in the mouse rather than normalized by individual organ. This optimization procedure prioritized organs with higher drug concentration and overall signal, which also enabled the model to converge faster and more consistently when implemented. The sampling ranges of these refined drug-retention coefficients (Kp_x) were reasonably close to the initial guess from AUC ratios (most well within $\pm 50\%$). After the parameter sets had been sorted according to the lowest least-squares error, the top 10 predictions based on LHS randomized parameter selection tracked with the data (Figure 2.3). The optimal parameter set for each mouse was selected from these candidate sets.

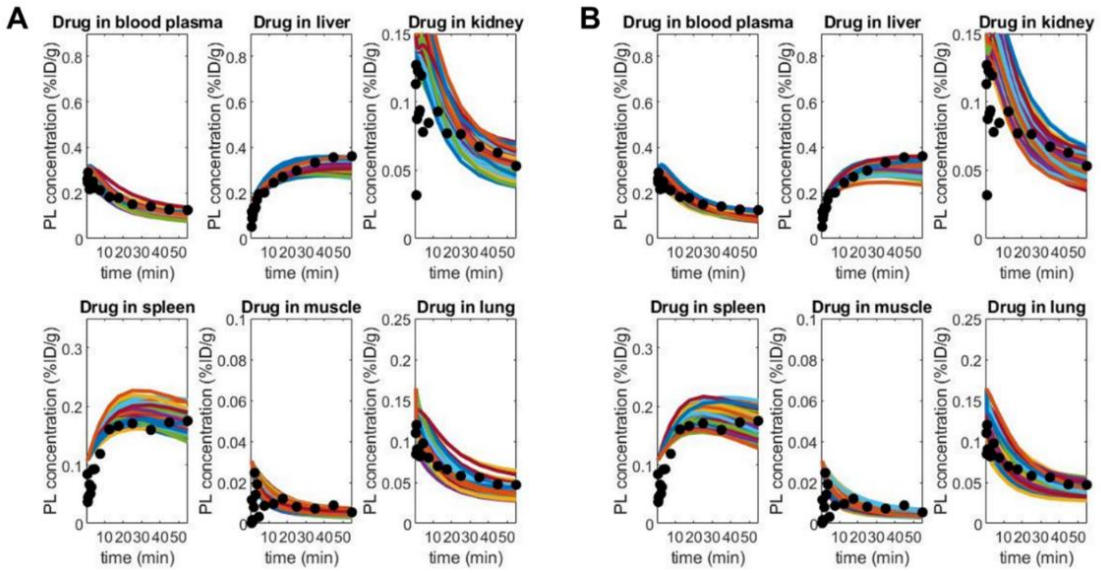

Figure 2.1. ***In Vivo*** **Experiment and PBPK Model Comparisons for a Full LHS Run.** Data (black dots) show PEGylated liposome (PL) drug concentrations in 6 compartments (blood plasma and 5 primary organs) of one APA+ mouse and are obtained via continuous PET/CT scan for the first hour after injection of drug. Simulated data (colored curves) are from the PBPK model, where the 2 sets of 100 trajectories shown (A and B) come from two rounds of simulations using parameter sets within the optimal ranges identified by Latin Hypercube Sampling (LHS).

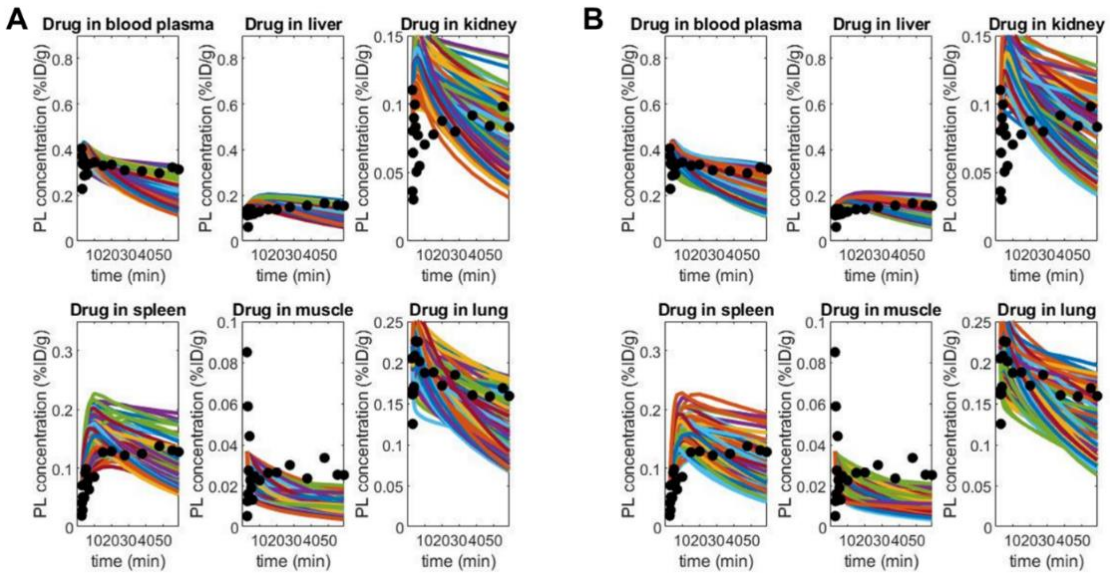

Figure 2.2. ***In Vivo*** **Experiment and PBPK Model Comparisons for a Full LHS Run.** Data (black dots) show PEGylated liposome (PL) drug concentrations in 6 compartments (blood plasma and 5 primary organs) of one naïve mouse and are obtained via continuous PET/CT scan for the first hour after injection of drug. Simulated data (colored curves) are from the PBPK model, where the 2 sets of 100 trajectories shown (A and B) come from two rounds of simulations using parameter sets within the wide ranges which were later refined by subsequent rounds of Latin Hypercube Sampling (LHS).

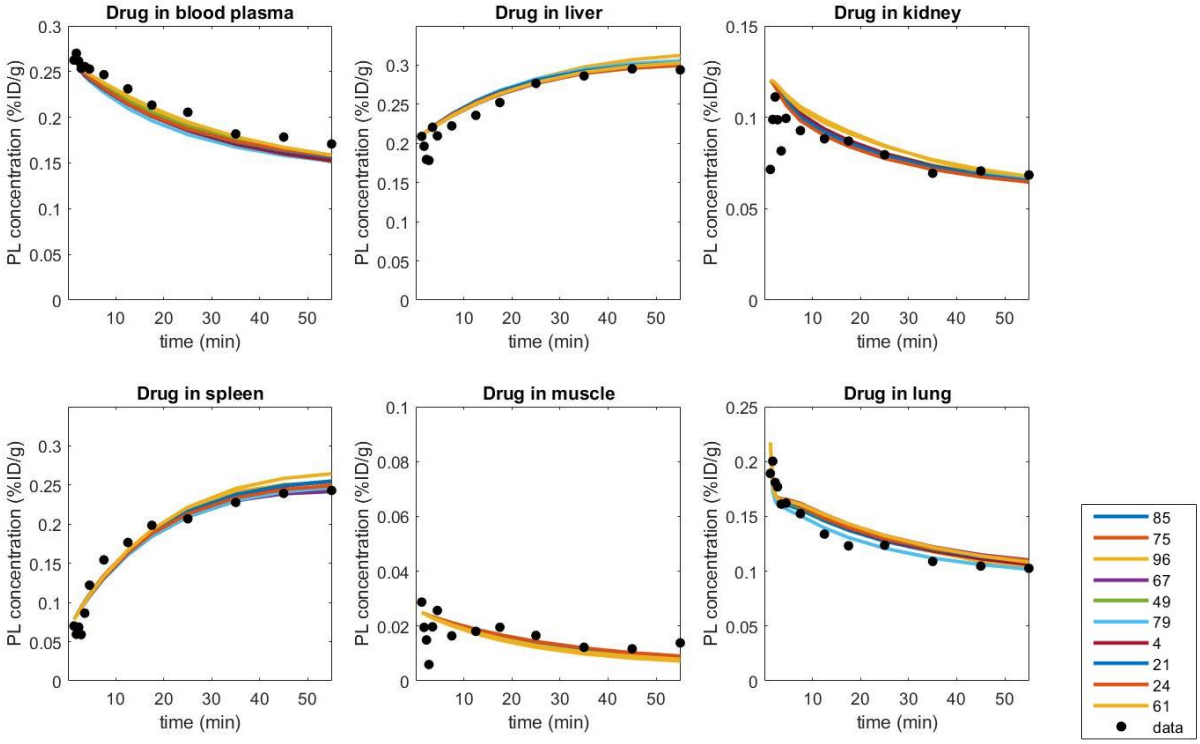

Figure 2.3. ***In Vivo*** **Experiment and PBPK Model Comparisons.** Data (black dots) show PL concentrations in 6 compartments (blood plasma and 5 primary organs) of one APA+ mouse, obtained via continuous PET/CT scan for the first hour after PL injection. Simulated data using the 10 most suitable parameter sets within the optimal ranges identified by LHS are overlaid with the experimental measurements (colored curves, with each color representing a unique LHS simulation ID).

Parametrizing the Model – an Exploration of Parameter Space

Since prolonged drug circulation typically correlates with improved efficacy, we focused on the altered clearance of PL between these cohorts. We next sought to specifically characterize which process(es) and compartment(s) in the PBPK model (and corresponding physiological processes) can distinguish drug clearance to the highest degree between cohorts of mice with and without APA.

Evidence suggests that the systemic clearance of PL and small immune complexes, such as PL bound to APA, is predominantly liver-mediated [24, 32, 33], in good agreement with our experimental and model findings that the organ with greatest PL accumulation over time is the liver. To explore this in greater detail, we focused simulations on the parameters responsible for controlling the extent of drug exposure and retention in the liver: the liver permeability fraction, fr_{li}, and the retention coefficient, Kp_{li}. Together, the parameters fr_{li} and Kp_{li} control total drug in the liver.

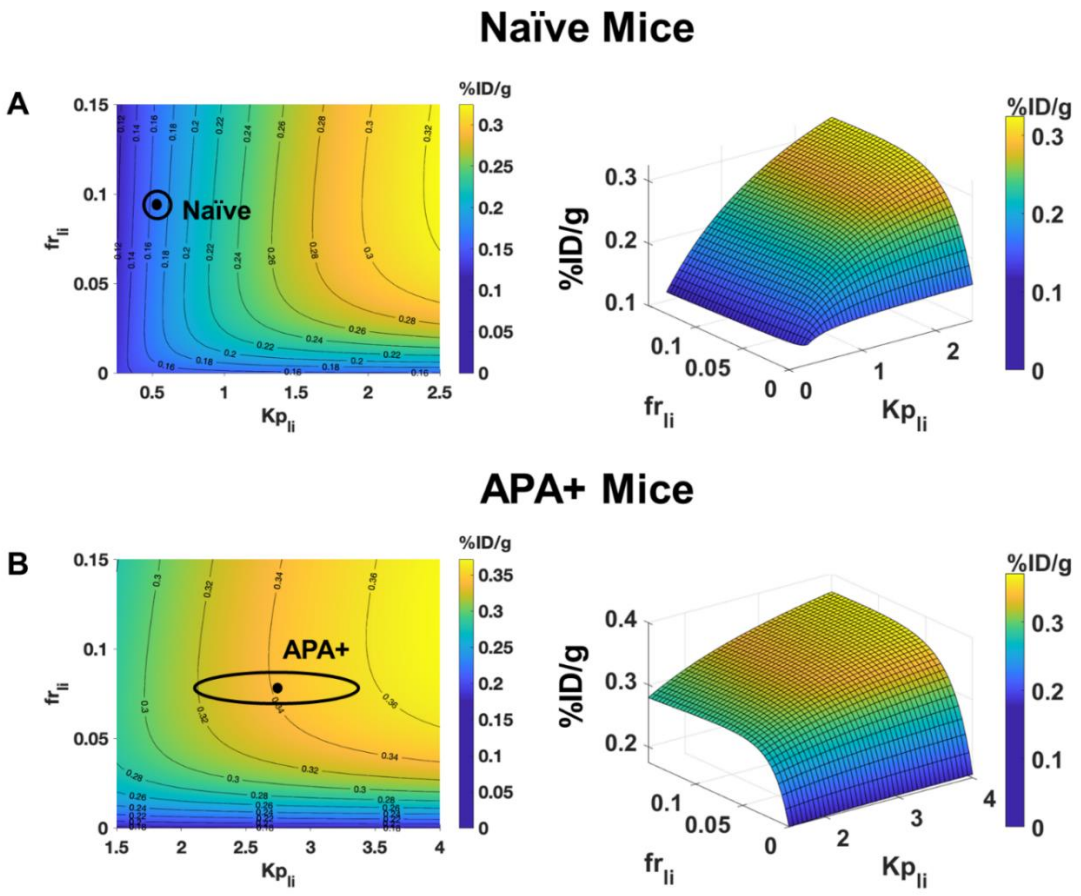

Figure 2.4. PBPK-Generated Heat Map of Drug Concentration in Liver at 1 Hour Post Injection Versus Liver Permeability (fr_{li}) and Liver Retention (Kp_{li}) Parameter Specifications. Ranges of parameters are identified from Latin Hypercube Sampling (LHS) based on experimental measurements for 1 hour post PEGylated liposome injection, from representative (A) naïve and (B) APA+ mice. All other PBPK model parameters are set at the average of optimal LHS-identified values for each cohort. The black dots are mean values of both liver parameters optimized by LHS based on best-fits to the experimental data over the entire 1-hour measurements, whereas the ellipses have semi-axes given by the standard deviations of each LHS-identified parameter for each cohort. Heat map colors and values are normalized so that 1 = 100 %ID/g.

We considered the concentration of PL in the liver as a measurement of percent injected dose per gram liver tissue (%ID/g). We measured uptake one hour post-injection, consistent with the early-phase redistribution of the liposomes and the available data for continuous PET/CT scanning. We conducted a parameter sweep for liver-specific *fr* and *Kp*, through the

widest region searched with LHS, while fixing the other parameters at the average of their optimized values (generating the prediction with the lowest least-squares error) for representative naïve and APA+ mice according to the characteristic LHS runs, and thus generated a space of simulated liver uptake in an "average mouse" for each cohort one hour after liposome injection (Figure 2.4). Here, we visualize LHS-identified parameter ranges for liver permeability (fr_{li}) and retention (Kp_{li}), and the LHS-identified best-fit values of both liver parameters from the experimental data over 1 hour for naive and APA+ mice. In this state diagram, we observe regions of parameter sensitivity and impact. Assuming a base level of drug availability (fr_{li}), there is consistently a gradient of PL taken up by the liver, increasing while Kp_{li} is increased. However, distinct regions emerge as fr_{li} is varied from its lower to upper bounds, occurring at the ridge where contour lines switch from horizontal to vertical (Figure 2.4). This implies that given sufficient permeability of the drug in the liver (through fr_{li} above a sufficiently high threshold), the final liver PL concentration loses sensitivity to fr_{li}, and liver drug concentration is driven primarily by the organ's ability to retain the PL (determined by Kp_{li}). At the far left of the landscape, for low Kp_{li}, liver retention is sufficiently low such that permeability (fr_{li}) makes no difference in overall uptake, since very little drug is retained regardless of availability.

When the model was optimized for the experimental data, all mice showed sufficient fr_{li} above the minimal threshold, and all naïve mice clustered on the far left of the landscape. Thus, both naïve and APA+ mice fall in the regions where Kp_{li} is a more sensitive parameter than fr_{li} in governing liver uptake. In other words, uptake in the liver compartment is driven more by its retention ability (partitioning coefficient Kp_{li}), and loses dependence on permeability after a certain point. In this framework, permeability simply controls how quickly the uptake occurs, but not total accumulation. For example, if Kp_{li} is fixed at a high value (assume, for instance,

Kp_{li} > 3), fr_{li} close to 1 will result in the drug uptake reaching the organ's "carrying capacity" (determined by Kp_{li}) almost immediately, within the first few minutes, whereas fr_{li} < 0.1 will result in the drug concentration gradually reaching its upper limit over the course of an hour. The liver retention coefficient (Kp_{li}) has similarly been identified as a critical parameter in the context of PBPK models for other therapeutics [34]. Correspondingly, we also find that if the retention ability and capacity to take up a drug are high enough, the availability of the PL determined by fr_{li} then becomes the factor limiting uptake and we see a rapidly increasing gradient as fr_{li} increases. Ultimately, if Kp_{li} and fr_{li} are sufficiently high (in the top right corner in Figure 2.4), we reach the upper bound of drug uptake in the liver. This "plateau" is limited only by the amount of drug in the body.

Physiologically, these findings suggest that a heightened drug retention in the liver (likely due to APA-mediated uptake into cells in the liver) is more responsible for increased concentration of PL in the liver in mice with APA, rather than drug permeability of the liver tissue or any changes to permeability promoting extravasation in the APA+ cohort. This is not surprising, as hepatic clearance is consistent with the elimination of small immune complexes from the circulation by liver sinusoidal endothelial cells expressing the receptor FcγIIb, which binds to the Fc domain of the PL-bound APA.

We next investigated other methods to confirm the liver drug retention capability Kp_{li} as the key parameter in differentiating the biodistribution patterns of PL in mice with distinct levels of APA. We examined the full parameter space and found that the parameters cluster for the mice within each cohort, with small fluctuations. Furthermore, in all drug retention (Kp_x) and permeability (fr_x) parameters, except for drug retention in the liver and spleen, there is no notable cohort-to-cohort difference as opposed to variation between individuals within a cohort; i.e.,

variability due to liver and spleen retention (Kp_{li}, Kp_s) is only notable in the presence of APA. This suggests APA+ and naïve mice otherwise appear physiologically similar (Figure 2.5, Table 2.1) (figure format adapted from [35]). Organ-specific *Kp* (drug retention ability) parameters optimized by LHS cluster consistently at small values (< 0.5) with the exception of liver- and spleen-specific *Kp* in APA+ mice. Kp_{li} and Kp_s are the most variable parameters, and the variability increases with the presence of APA (Figure 2.5A). Organ-specific *fr* (extent of permeability) parameters are consistently optimized around 0.1 in all mice, regardless of APA status. Thus, drug permeability (*fr*) parameters have low variability relative to drug retention (*Kp*) parameters and are not influenced by the presence of APA (Figure 2.5B).

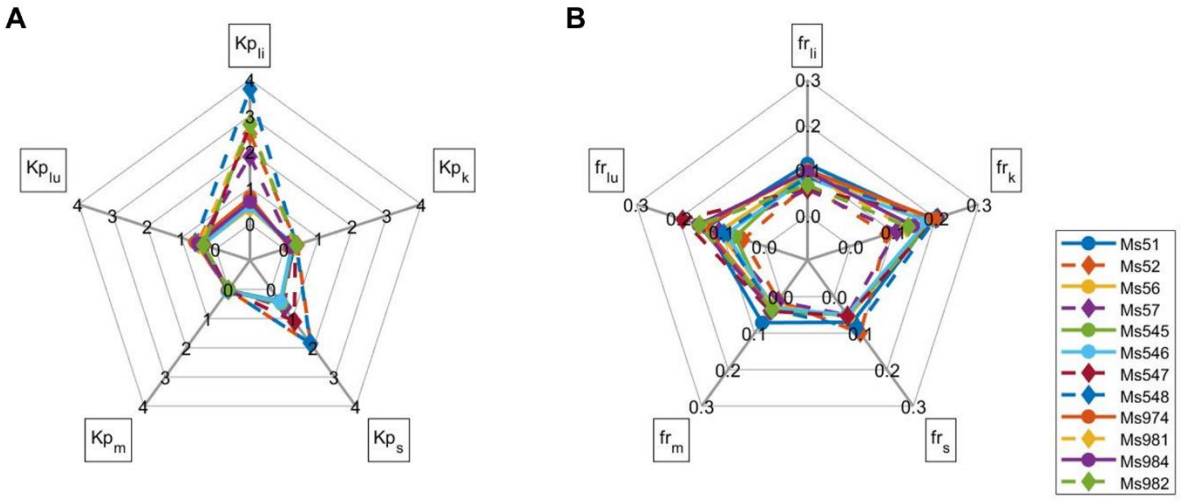

Figure 2.5. Spider Plots of LHS-Optimized Parameters. (A) Retention and (B) permeability parameters for all 5 primary organs from 12 mice. Each colored line represents an individual mouse (diamonds and dashed lines indicate mice with APA and circles and solid lines indicate naïve mice). Note that spleen data are not available for 4 of the mice.

While spleen data were unavailable for 4 of the mice in the sample set due to inability to accurately delineate the spleen in PET/CT imaging, gamma counter readings at the terminal time point confirm a high splenic concentration. Isolating and looking more closely at retention

coefficients for liver and spleen, we can quantify a significant disparity in the behavior of these optimal parameters dependent on whether or not a mouse has high APA (Figure 2.6). These liver (Kp_{li}) and spleen (Kp_s) retention parameters were the optimal parameters identified for each mouse when optimized by LHS according to our experimental system of continuously tracking PL distribution for 1 hour. We find that optimal liver and spleen retention parameters are indeed correlated with APA status: both are significantly larger ($p < 0.05$: unpaired, one-tailed t-test with Welch's correction) and more variable ($p < 0.05$: F test) in APA+ mice. This further suggests that both liver (primary) and spleen (secondary) retention are responsible for the disparity in mechanisms underlying accelerated blood clearance of PL between the different mouse cohorts. Physiologically, this points to crosslinking by APA to create PL, APA, liver/spleen species complexes as the primary mechanism by which APA alters biodistribution.

Table 2.1. Ranges of All Optimized Permeability and Retention Parameters. Ranges reflect optimized values for each unknown permeability (*fr*) and retention (*Kp*) parameter reported for all 12 individual mice in the study. The increased range and stratification between naïve and APA+ mice for Kp_{li} and Kp_s are highlighted in bold.

Parameter	Total Range	Naïve Range	APA+ Range
fr_{li}	0.057-0.113	0.083-0.113	0.057-0.093
fr_k	0.085-0.204	0.146-0.196	0.085-0.204
fr_s	0.050-0.100	0.050-0.070	0.050-0.100
fr_m	0.011-0.072	0.026-0.072	0.011-0.040
fr_{lu}	0.050-0.192	0.069-0.155	0.050-0.192
$\boldsymbol{Kp_{li}}$	**0.435-3.744**	**0.435-0.734**	**1.869-3.744**
Kp_k	0.160-0.379	0.160-0.308	0.230-0.379
$\boldsymbol{Kp_s}$	**0.413-1.867**	**0.413-0.484**	**0.614-1.867**
Kp_m	0.009-0.063	0.013-0.063	0.009-0.030
Kp_{lu}	0.333-0.603	0.365-0.590	0.333-0.603

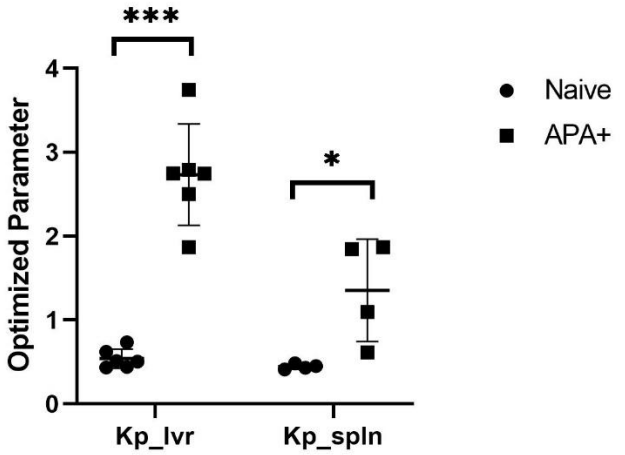

Figure 2.6. Correlations Between Liver and Spleen LHS-Optimized Retention Parameters. Values corresponding to APA+ mice (n=6 in liver, n=4 in spleen) are presented as circles and values corresponding to naïve mice (n=6 in liver, n=4 in spleen) are presented as squares. Error bars represent standard deviations. (*$p < 0.05$, ***$p < 0.001$).

Discussion

PEG is routinely conjugated to proteins and liposomes to reduce the immunogenicity and extend the systemic circulation times of the underlying therapeutic [26]. There are currently at least 12 PEGylated therapeutics on the market, and many more in development [26]. Unfortunately, evidence has emerged that some patients may possess pre-existing or develop APA, which in turn leads to ABC of select PEGylated therapeutics [36, 37], including Krystexxa [38, 39] and Oncospar [40]. Animal studies have repeatedly shown that APA can lead to ABC of PL [24, 33, 41]. There are even suspicions that APA may be responsible for the anaphylactic response to COVID-19 mRNA vaccines formulated with PEG-lipids [42, 43]. Thus, there is immense interest in a better understanding of how APA can engage PEGylated drugs in living systems, and the consequent temporal fate of the PEGylated drug. While *in vivo* studies have elucidated the immunological mechanisms of the APA induction [33], the ABC phenomenon

[25, 44], and the resulting biodistribution of the PEGylated drugs, these existing studies do not readily reveal the key physiological mechanisms that are responsible for the clearance itself.

Here, by performing search and optimization using Latin Hypercube Sampling on an 8-compartment PBPK model together with PET/CT data, we identify the most influential factors that drive the observed accumulation of PL/APA complexes in the liver and spleen. Our work gives insight into the physiological factors underlying the PBPK model for PEGylated nanomedicine biodistribution, refines the parameter unknowns from experimental data, and explains the observed variation in the system. In this way, we gain mechanistic insights into accelerated drug clearance by APA that are otherwise difficult to measure and validate experimentally.

In the model, consistent with PET/CT studies, we observed naïve mice exhibited less variability in their optimized parametrizations and maintained nearly constant signals through the first hour. This contrasts with the greater variations in mice with appreciable APA titers, which underscores the complexity of APA-mediated ABC. The liver and spleen ability to retain the PL drug carriers (high retention coefficients Kp_{li}, Kp_{s}) exhibited the most significant difference between the naïve and APA+ cohorts and subsequently appeared to be the driving parameters in this system, distinguishing the cohorts of mice with and without APA. The liver and spleen permeability to PLs, controlled by fr_{li}, $fr_{s,}$ restrict the amount of drug accessible to the liver and spleen; these properties are not greatly affected by APA status, indicating that, mechanistically, the difference in clearance driven by APA is attributed to APA binding to PL and retaining it in the liver once extravasated as APA/PL immunocomplexes (e.g., via affinity to LSECs or Kupffer cells, found in the tissue/interstitial sub-compartment). However, the APA do not necessarily speed the process of exposing the liver to the drug, which would be a process limited by delivery

via blood flow or capillary permeability and reflected in greater sensitivity to drug permeability. This was not the case reflected in the model or the data. Increased total drug uptake in the liver and spleen is further evidenced in comparing the time series for PET signal and AUC values between the cohorts. We have identified that the retention process in the liver, attributed in the model to Kp_{li} and caused physiologically by antibodies cross-linking PL in the liver, is primarily responsible for the increased liver uptake. This is the greatest difference between the mice in the APA+ vs. naïve cohorts.

We acknowledge that the model system has a large number of parameters, and there is always a possibility of multiple optimal parameter ranges consistent with the experimental data. However, we are encouraged by the consistent clustering between mice and the ability of LHS to distinguish naïve and APA+ mice by their non-overlapping ranges for liver and spleen permeation and retention properties, while also revealing greater variability in APA+ mice. While other approaches to parameter estimation, such as Markov Chain Monte Carlo, have been demonstrated for other dynamical systems [45, 46], LHS was able to afford valuable insights at a reduced computational cost.

Overall, these data-based analyses provide a means to further our understanding of the driving physiological processes behind accelerated clearance, and to begin to consider strategies for overcoming APA-mediated accelerated clearance.

Acknowledgments

The authors would like to thank Morgan McSweeney for the meaningful discussions contributing to this work. We would also like to thank the staff at the Biomedical Research Imaging Center and Animal Studies Core at the University of North Carolina at Chapel Hill.

REFERENCES

[1] R.P. Brown, M.D. Delp, S.L. Lindstedt, L.R. Rhomberg, R.P. Beliles, Physiological parameter values for physiologically based pharmacokinetic models, Toxicology and industrial health, 13 (1997) 407-484.

[2] B. Davies, T. Morris, Physiological Parameters in Laboratory Animals and Humans, Pharmaceutical Research, 10 (1993) 1093-1095.

[3] A. Garg, J.P. Balthasar, Physiologically-based pharmacokinetic (PBPK) model to predict IgG tissue kinetics in wild-type and FcRn-knockout mice, Journal of Pharmacokinetics and Pharmacodynamics, 34 (2007) 687-709.

[4] N. Kaliss, D. Pressman, Plasma and blood volumes of mouse organs, as determined with radioactive iodoproteins, Proceedings of the Society for Experimental Biology and Medicine. Society for Experimental Biology and Medicine (New York, N.Y.), 75 (1950) 16-20.

[5] Y. Huh, D.E. Smith, M. Rose Feng, Interspecies scaling and prediction of human clearance: comparison of small- and macro-molecule drugs, Xenobiotica, 41 (2011) 972-987.

[6] J. Mordenti, S.A. Chen, J.A. Moore, B.L. Ferraiolo, J.D. Green, Interspecies Scaling of Clearance and Volume of Distribution Data for Five Therapeutic Proteins, Pharmaceutical Research, 8 (1991) 1351-1359.

[7] W.A. Ritschel, N.N. Vachharajani, R.D. Johnson, A.S. Hussain, The allometric approach for interspecies scaling of pharmacokinetic parameters, Comparative Biochemistry and Physiology Part C: Comparative Pharmacology, 103 (1992) 249-253.

[8] H.M. Jones, K. Rowland-Yeo, Basic Concepts in Physiologically Based Pharmacokinetic Modeling in Drug Discovery and Development, CPT: Pharmacometrics & Systems Pharmacology, 2 (2013) 63.

[9] D. Yuan, H. He, Y. Wu, J. Fan, Y. Cao, Physiologically Based Pharmacokinetic Modeling of Nanoparticles, Journal of Pharmaceutical Sciences, 108 (2019) 58-72.

[10] F. Stader, M. Battegay, C. Marzolini, Physiologically based pharmacokinetic modelling to support the clinical management of drug-drug interactions with bictegravir, Clinical pharmacology and therapeutics, (2021).

[11] T. Ueno, Y. Miyajima, I. Landry, B. Lalovic, E. Schuck, Physiologically Based Pharmacokinetic Modeling to Predict Drug Interactions of Lemborexant with CYP3A Inhibitors, CPT Pharmacometrics Syst Pharmacol, (2021).

[12] J. Lang, L. Vincent, M. Chenel, K. Ogungbenro, A. Galetin, Impact of Hepatic CYP3A4 Ontogeny Functions on Drug-Drug Interaction Risk in Pediatric Physiologically-Based Pharmacokinetic/Pharmacodynamic Modeling: Critical Literature Review and Ivabradine Case Study, Clinical pharmacology and therapeutics, (2020).

[13] J.D. Lutz, A. Mathias, P. German, C. Pikora, S. Reddy, B.J. Kirby, Physiologically-Based Pharmacokinetic Modeling of Remdesivir and its Metabolites to Support Dose Selection for the Treatment of Pediatric Patients with COVID-19, Clinical pharmacology and therapeutics, (2021).

[14] J. Fan, X. Zhang, L. Zhao, Utility of Physiologically Based Pharmacokinetic Absorption Modeling to Predict the Impact of Salt-to-Base Conversion on Prasugrel HCl Product Bioequivalence in the Presence of Proton Pump Inhibitors, The AAPS journal, 19 (2017) 1479-1486.

[15] M. Le Merdy, J. Spires, V. Lukacova, M.L. Tan, A. Babiskin, X. Xu, L. Zhao, M.B. Bolger, Ocular Physiologically Based Pharmacokinetic Modeling for Ointment Formulations, Pharm Res, 37 (2020) 245.

[16] Y. Cao, W.J. Jusko, Applications of minimal physiologically-based pharmacokinetic models, J Pharmacokinet Pharmacodyn, 39 (2012) 711-723.

[17] H. He, C. Liu, Y. Wu, X. Zhang, J. Fan, Y. Cao, A Multiscale Physiologically-Based Pharmacokinetic Model for Doxorubicin to Explore its Mechanisms of Cytotoxicity and Cardiotoxicity in Human Physiological Contexts, Pharm Res, 35 (2018) 174.

[18] H. He, D. Yuan, Y. Wu, Y. Cao, Pharmacokinetics and Pharmacodynamics Modeling and Simulation Systems to Support the Development and Regulation of Liposomal Drugs, Pharmaceutics, 11 (2019).

[19] R. Nasu, Y. Kumagai, H. Kogetsu, M. Tsujimoto, H. Ohtani, Y. Sawada, Physiologically based pharmacokinetic model for pralmorelin hydrochloride in rats, Drug metabolism and disposition: the biological fate of chemicals, 33 (2005) 1488-1494.

[20] C. Walsh, J.J. Bonner, T.N. Johnson, S. Neuhoff, E.A. Ghazaly, J.G. Gribben, A.V. Boddy, G.J. Veal, Development of a physiologically based pharmacokinetic model of actinomycin D in children with cancer, British journal of clinical pharmacology, 81 (2016) 989-998.

[21] A.N. Edginton, E.I. Zimmerman, A. Vasilyeva, S.D. Baker, J.C. Panetta, Sorafenib metabolism, transport, and enterohepatic recycling: physiologically based modeling and simulation in mice, Cancer Chemotherapy and Pharmacology, 77 (2016) 1039-1052.

[22] M. Krauss, R. Burghaus, J. Lippert, M. Niemi, P. Neuvonen, A. Schuppert, S. Willmann, L. Kuepfer, L. Görlitz, Using Bayesian-PBPK modeling for assessment of inter-individual variability and subgroup stratification, In Silico Pharmacol, 1 (2013) 6-6.

[23] N. Tsamandouras, A. Rostami-Hodjegan, L. Aarons, Combining the ‘bottom up’ and ‘top down’ approaches in pharmacokinetic modelling: fitting PBPK models to observed clinical data, British Journal of Clinical Pharmacology, 79 (2015) 48-55.

[24] M.D. McSweeney, T. Wessler, L.S.L. Price, E.C. Ciociola, L.B. Herity, J.A. Piscitelli, W.C. Zamboni, M.G. Forest, Y. Cao, S.K. Lai, A minimal physiologically based pharmacokinetic

model that predicts anti-PEG IgG-mediated clearance of PEGylated drugs in human and mouse, Journal of Controlled Release, 284 (2018) 171-178.

[25] A.S. Abu Lila, H. Kiwada, T. Ishida, The accelerated blood clearance (ABC) phenomenon: Clinical challenge and approaches to manage, Journal of Controlled Release, 172 (2013) 38-47.

[26] Q. Yang, S.K. Lai, Anti-PEG immunity: emergence, characteristics, and unaddressed questions, Wiley interdisciplinary reviews. Nanomedicine and nanobiotechnology, 7 (2015) 655-677.

[27] M.D. McKay, R.J. Beckman, W.J. Conover, A Comparison of Three Methods for Selecting Values of Input Variables in the Analysis of Output from a Computer Code, Technometrics, 21 (1979) 239-245.

[28] R.L. Iman, J.C. Helton, J.E. Campbell, An Approach to Sensitivity Analysis of Computer Models: Part I—Introduction, Input Variable Selection and Preliminary Variable Assessment, Journal of Quality Technology, 13 (1981) 174-183.

[29] J.C. Helton, F.J. Davis, Latin hypercube sampling and the propagation of uncertainty in analyses of complex systems, Reliability Engineering & System Safety, 81 (2003) 23-69.

[30] S.C. Hora, R.L. Iman, Expert Opinion in Risk Analysis: The NUREG-1150 Methodology, Nuclear Science and Engineering, 102 (1989) 323-331.

[31] S. Marino, I.B. Hogue, C.J. Ray, D.E. Kirschner, A methodology for performing global uncertainty and sensitivity analysis in systems biology, Journal of Theoretical Biology, 254 (2008) 178-196.

[32] L.P. Ganesan, J. Kim, Y. Wu, S. Mohanty, G.S. Phillips, D.J. Birmingham, J.M. Robinson, C.L. Anderson, FcγRIIb on liver sinusoidal endothelium clears small immune complexes, J Immunol, 189 (2012) 4981-4988.

[33] T. Ishida, M. Harada, X.Y. Wang, M. Ichihara, K. Irimura, H. Kiwada, Accelerated blood clearance of PEGylated liposomes following preceding liposome injection: Effects of lipid dose and PEG surface-density and chain length of the first-dose liposomes, Journal of Controlled Release, 105 (2005) 305-317.

[34] N.H. Hsieh, B. Reisfeld, F.Y. Bois, W.A. Chiu, Applying a Global Sensitivity Analysis Workflow to Improve the Computational Efficiencies in Physiologically-Based Pharmacokinetic Modeling, Frontiers in pharmacology, 9 (2018) 588.

[35] Moses, spider_plot (https://github.com/NewGuy012/spider_plot), in: GitHub, 2021.

[36] T.J. Povsic, M.G. Lawrence, A.M. Lincoff, R. Mehran, C.P. Rusconi, S.L. Zelenkofske, Z. Huang, J. Sailstad, P.W. Armstrong, P.G. Steg, C. Bode, R.C. Becker, J.H. Alexander, N.F. Adkinson, A.I. Levinson, Pre-existing anti-PEG antibodies are associated with severe immediate allergic reactions to pegnivacogin, a PEGylated aptamer, Journal of Allergy and Clinical Immunology, 138 (2016) 1712-1715.

[37] G.T. Kozma, T. Shimizu, T. Ishida, J. Szebeni, Anti-PEG antibodies: Properties, formation, testing and role in adverse immune reactions to PEGylated nano-biopharmaceuticals, Advanced Drug Delivery Reviews, (2020).

[38] M.S. Hershfield, N.J. Ganson, S.J. Kelly, E.L. Scarlett, D.A. Jaggers, J.S. Sundy, Induced and pre-existing anti-polyethylene glycol antibody in a trial of every 3-week dosing of pegloticase for refractory gout, including in organ transplant recipients, Arthritis Research & Therapy, 16 (2014) R63.

[39] P.E. Lipsky, L.H. Calabrese, A. Kavanaugh, J.S. Sundy, D. Wright, M. Wolfson, M.A. Becker, Pegloticase immunogenicity: the relationship between efficacy and antibody development in patients treated for refractory chronic gout, Arthritis Research & Therapy, 16 (2014) R60.

[40] J.K. Armstrong, G. Hempel, S. Koling, L.S. Chan, T. Fisher, H.J. Meiselman, G. Garratty, Antibody against poly(ethylene glycol) adversely affects PEG-asparaginase therapy in acute lymphoblastic leukemia patients, Cancer, 110 (2007) 103-111.

[41] M. Mohamed, A.S. Abu Lila, T. Shimizu, E. Alaaeldin, A. Hussein, H.A. Sarhan, J. Szebeni, T. Ishida, PEGylated liposomes: immunological responses, Science and Technology of Advanced Materials, 20 (2019) 710-724.

[42] J. Kleine-Tebbe, L. Klimek, E. Hamelmann, O. Pfaar, C. Taube, M. Wagenmann, T. Werfel, M. Worm, Severe allergic reactions to the COVID-19 vaccine - statement and practical consequences, Allergol Select, 5 (2021) 26-28.

[43] M. Worm, A. Bauer, B. Wedi, R. Treudler, W. Pfuetzner, K. Brockow, T. Buhl, T. Zuberbier, J. Fluhr, G. Wurpts, L. Klimek, T. Jacob, H.F. Merk, N. Mülleneisen, S. Roeseler, H. Dickel, U. Raap, J. Kleine-Tebbe, Practical recommendations for the allergological risk assessment of the COVID-19 vaccination - a harmonized statement of allergy centers in Germany, Allergol Select, 5 (2021) 72-76.

[44] T. Ishida, H. Kiwada, [Accelerated blood clearance (ABC) phenomenon induced by administration of PEGylated liposome], Yakugaku zasshi : Journal of the Pharmaceutical Society of Japan, 128 (2008) 233-243.

[45] C. Li, Y. Pei, M. Zhu, Y. Deng, Parameter Estimation on a Stochastic SIR Model with Media Coverage, Discrete Dynamics in Nature and Society, 2018 (2018) 3187807.

[46] A.S. Talawar, U.R. Aundhakar, Parameter Estimation of SIR Epidemic Model Using MCMC Methods, Global Journal of Pure and Applied Mathematics, 12 (2016).

CHAPTER 3: HIGH MW PEG RESTORES PROLONGED CIRCULATION OF KRYSTEXXA IN MICE WITH ANTI-PEG ANTIBODIES[3]

Summary

Krystexxa® (PEG-uricase) is an enzyme used to reduce serum uric acid levels in patients with chronic, treatment-refractory gout. Clinically, about 40% of patients develop anti-PEG antibodies (APA) after initial treatment, which in turn quickly eliminate subsequent doses of Krystexxa from the systemic circulation and render the treatment ineffective. We previously found that pre-infusion with high MW free PEG (40 kDa) can serve as a decoy to saturate circulating APA, preventing binding to a subsequently administered dose of PEG-liposomes and restoring their prolonged circulation in mice, without any detectible toxicity. Here, we investigated the use of 40 kDa free PEG to restore the circulation of radio-labeled Krsytexxa in mice using longitudinal Positron Emission Tomography (PET) imaging over 4 days. Mice injected with Krystexxa developed appreciable APA titers by Day 9, which further increased through Day 14. Compared to naïve mice, mice with Krystexxa-induced APA rapidly cleared ^{89}Zr-labeled Krystexxa, with ~75% lower Krystexxa levels in the circulation within the first four hours, and the bulk of the drug cleared to the liver and spleen within 24 hrs. In contrast, pre-infusion of free PEG into PEG-sensitized mice restored the AUC of PEG-uricase to ~80% of that seen in naïve mice, resulting in a similar biodistribution to Krystexxa in naïve mice over time.

[3] This chapter is adapted from a preprint of an article submitted to the Journal of Controlled Release. The original citation is as follows:
Talkington A.M., McSweeney M.D., Zhang T., Li Z., Nyborg A., Livingston E.W., Frank J.E., Yuan H., Lai S.K. "High MW PEG restores prolonged circulation of Krystexxa in mice with anti-PEG antibodies," Journal of Controlled Release (submitted).

These results suggest that pre-infusion of free PEG may be a promising strategy to enable the safe and efficacious use of Krystexxa in patients that have previously failed therapy due to induced APA.

Introduction

Krystexxa®, a PEGylated uricase enzyme comprised of roughly five molecules of 10 kDa PEG chains conjugated to each uricase molecule [1], is currently the only FDA-approved treatment for severe, treatment-refractory chronic gout, a type of inflammatory arthritis affecting ~25,000-100,000 patients in the U.S. each year [2]. Its mechanism of action is based on the circulating uricase enzyme breaking down uric acid in the circulation, resulting in a gradual reduction or elimination of the tophi (uric acid crystals in the joint) responsible for the underlying inflammation with gout. Naturally, maintaining sustained serum levels of Krystexxa® adequate to suppress uric acid levels is essential for its efficacy, and represent the major reason why the treatment is administered by IV infusion every 2 weeks. Unfortunately, over 40% of patients treated with Krystexxa develop high titers of anti-PEG antibodies (APA) [3-7]. The induced APA lead to rapid elimination of Krystexxa from the systemic circulation, rendering the treatment ineffective [3] with no alternative interventions available for tens of thousands of patients in the U.S. each year.

Given the urgency of this challenge, a number of companies and investigators have sought to advance alternatives to Krystexxa. These interventions typically involve either modifying a uricase enzyme with different polymers [8-15], and/or combining a uricase molecule with some form of immunosuppression [16, 17]. When searching for a solution to overcome the challenges presented by APA, we were drawn to the safety and relative

immunological inertness of free PEG administered IV [18-23]. This contrasts to when PEG is conjugated to select proteins or liposomes, which can be inherently immunogenic [14, 22, 24, 25]. We hypothesized that the infusion of free-PEG could competitively inhibit pre-existing APA from binding PEGylated drugs, providing a safe, effective, and readily clinically translatable intervention that restores the safe and efficacious use of PEGylated drugs adversely impacted by APA. In support of our hypothesis, we found that in mice with APA levels matching high APA titers found in the general population, injection of 40 kDa free PEG increased the amount of circulating PEG-liposomes 48 hrs post-infusion by >100-fold compared to similarly PEG-sensitized mice treated with either PBS or 10 kDa free-PEG, restoring PEG-liposome concentrations to a level comparable to naïve mice with no APA [26]. Importantly, the toxicity profile of the chronic administration of free PEG to PEG-sensitized mice (including complete blood counts, renal function assays, and liver/kidney histology) were indistinguishable from control groups treated with PBS. More impressively, repeated dosing of free PEG did not stimulate additional APA secretion, even in mice that had been previously sensitized to produce APA, and a single dose of 40 kDa free PEG suppressed APA induction for 3 months [27].

Building off of these promising findings, we sought to investigate in this study whether infusion of 40 kDa free PEG would restore the efficacy of Krystexxa in the presence of Krystexxa-induced APA. The urate oxidase knockout mouse model is exceptionally difficult, and the pharmacokinetics (PK) profile of Krystexxa is highly predictive of its efficacy. Thus, we decided to evaluate the effectiveness of pre-infusion of 40 kDa free PEG in restoring the efficacy of Krystexxa by monitoring the PK profile of ^{89}Zirconium-labeled Krystexxa in real time using Positron Emission Tomography (PET) imaging in live animals. Similar to our earlier studies, we

found that pre-infusion of free PEG was an exceptionally simple yet effective means of restoring the prolonged systemic circulation of Krystexxa in mice with high titers of APA.

Results

Mouse model of Krystexxa-induced APA

Clinically, Krystexxa is administered via IV infusion once every 2 weeks, and APA-mediated rapid elimination of Krystexxa is often observed as quickly as by the second dose, implying that high APA titers are induced within 2 weeks of the first infusion [3]. Although Krystexxa-induced APA is readily apparent in clinical studies, its immunogenicity profile in mice is not well understood, as prior studies did not assess potential induction of APA. To mimic its use in humans, we injected Krystexxa via the tail vein into immunocompetent BALB/c mice on Day 0, and quantified anti-PEG IgG and IgM on both Day 9 and Day 14 (Figure 3.1A, B). In good agreement with clinical reports, we detected a considerable increase of IgG and IgM APA across this duration, with a rapid increase between Day 9 and Day 14 (Figure 3.1B, C). Indeed, anti-PEG IgG was increased from ~1.7 ± 0.9 μg/mL on Day 9 to ~10.4 ± 7.3 μg/mL by Day 14, whereas anti-PEG IgM was increased from ~0.4 ± 0.3 μg/mL on Day 9 to ~2.6 ± 2.3 μg/mL by Day 14. Our findings are consistent with the literature showing that anti-PEG immune response to pegloticase increases after 1 week [28]. These induced levels of APA by Krystexxa in mice parallels the highest levels of APA we had previously detected in blood samples from the general healthy population [29], but remains substantially lower than the APA levels induced by IV infusion of PEG-liposomes in mice [27, 30].

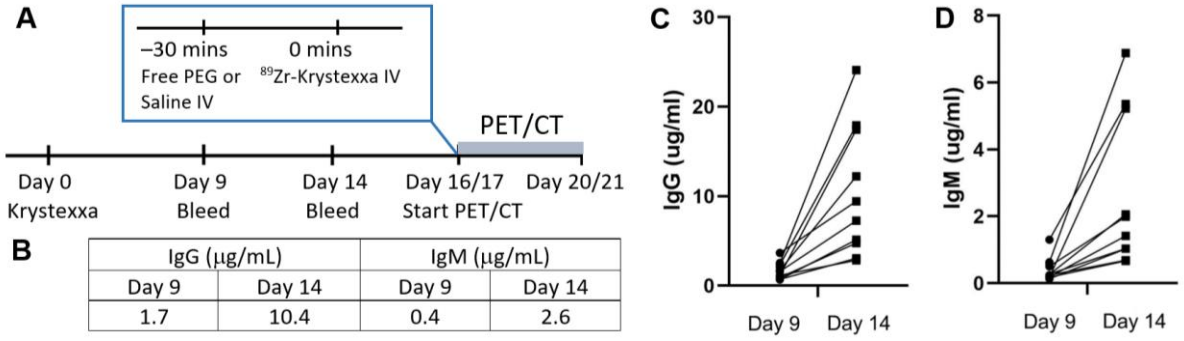

IgG (μg/mL)		IgM (μg/mL)	
Day 9	Day 14	Day 9	Day 14
1.7	10.4	0.4	2.6

Figure 3.1. Study Design and Induction of APA. (A) Study design and experimental timeline. (B) Average anti-PEG IgG and IgM in mice 9 and 14 days after initial Krystexxa infusion on Day 0. Changes in (C) IgG and (D) IgM APA levels in mice from Day 9 to Day 14.

PET imaging for assessing the PK profile of ^{89}Zr-labeled Krystexxa

After confirming that Krystexxa induced substantial APA titers within 2 weeks, we next performed a PET/CT study in the same animals assessing the impact of APA on the circulation of radiolabeled Krystexxa (Figure 3.2). We assigned APA+ mice randomly into two groups (placebo control vs. free PEG treated; Figure 3.3), and also included naïve Balb/c mice (i.e., not PEG-sensitized) that served as a negative control to represent the normal PK profile of Krystexxa. To assess the PK of Krystexxa in the same mice over time, Krystexxa was modified with chelator cheisothiocyanatobenzyl-desferrioxamine, which was then labeled with ^{89}Zr [31]. All mice received either saline or free PEG intravenously. 45 min later, mice were injected with a bolus of ^{89}Zr-Krystexxa (4.1±1.3 MBq), followed immediately with a 60 min dynamic PET scan. CT was conducted afterwards. Repeated PET/CT scans were conducted at 4, 24, 48, 72, and 96 hours post the injection of ^{89}Zr-Krystexxa. The group information was masked out during image acquisition and image analysis.

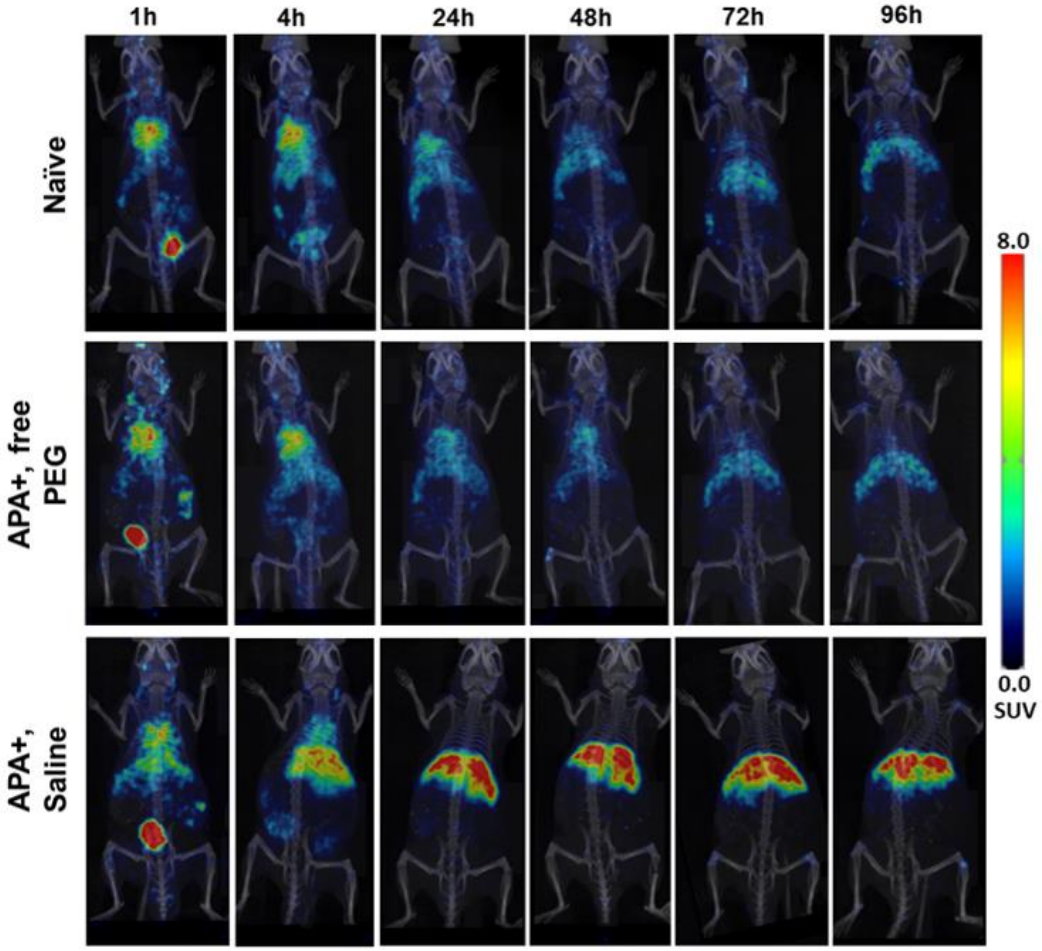

Figure 3.2. PET/CT Imaging of Mice. PET/CT imaging was performed at different time points to assess pharmacokinetics and biodistribution of ^{89}Zr-Krystexxa in 3 cohorts: naïve mice infused with saline before Krystexxa, PEG-sensitized (APA+) mice infused with free PEG prior to Krystexxa, and PEG-sensitized (APA+) mice infused with saline prior to Krystexxa. Single PET coronal sections were overlayed on CT MIP images to represent the distribution of ^{89}Zr-Krystexxa over time.

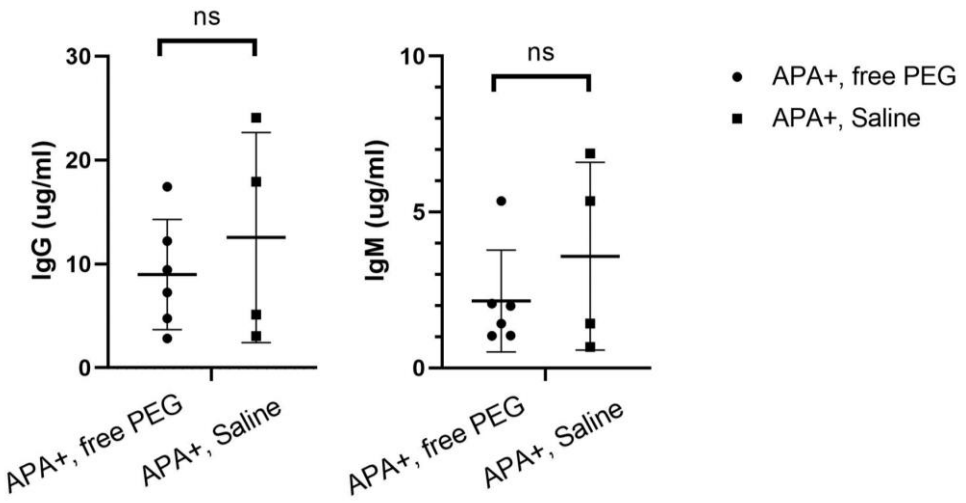

Figure 3.3. Distribution of Induced APA in Mice. Distribution (mean and SD) of induced (A) IgG and (B) IgM levels in all mice. IgG and IgM levels were not statistically different between the two groups (two-tailed Welch's t-test).

Almost immediately, the APA-mediated clearance was apparent in the APA+, saline-treated cohort, as evidenced by the steep downward trend in plasma Krystexxa levels in the first hour after injection, corresponding with an upward trend in hepatic Krystexxa signal (Figure 3.4A, B). In contrast, the plasma concentration of Krystexxa in the naïve and free PEG-treated APA+ cohorts remained at a much higher level. This trend continued and became even more pronounced by 4 hours post injection. Early clearance was notable in the kidney and lung in the APA+, saline-treated mice, with corresponding accumulation in the liver during the first 4 hours post injection (Figure 3.4C, D). This is consistent with prior reports suggesting that APA may mediate accelerated blood clearance through the formation of small immune complexes, driving FcgR11b-mediated clearance by liver sinusoidal endothelial cells [32], or through alternative activation of complement, broadly driving phagocyte-mediated clearance [33]. Signal in the muscle does not differ notably between the groups (Figure 3.4E).

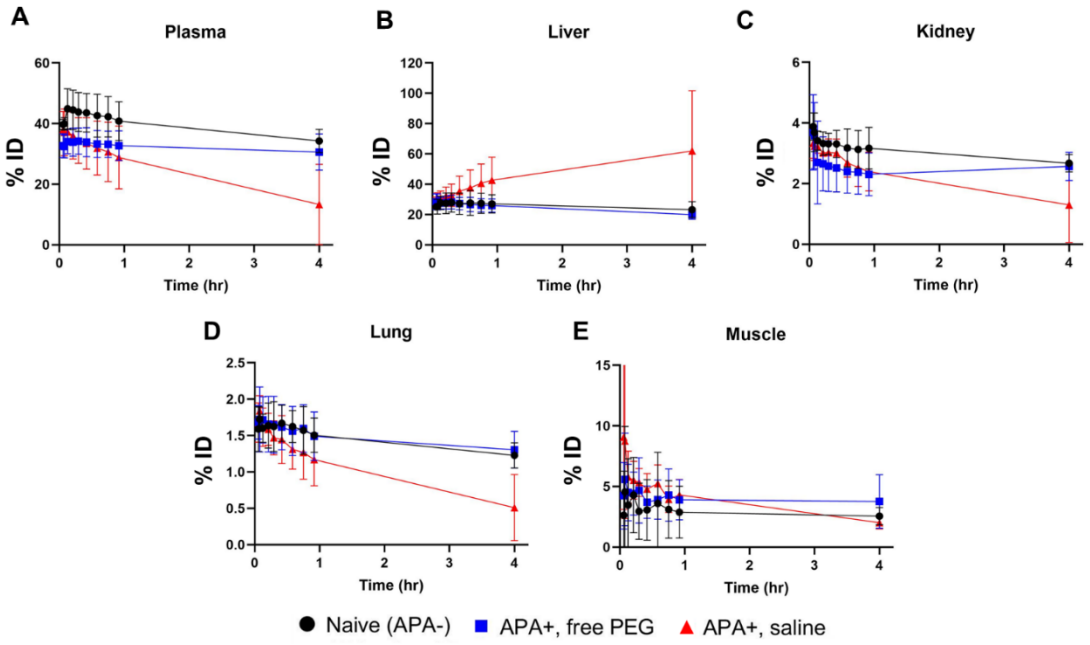

Figure 3.4. Mean Krystexxa Levels Through 4h. Mean Krystexxa levels over the first 4h in (A) plasma, (B) liver, (C) kidney, (D) lung, and (E) muscle, as determined by PET/CT imaging. Solid black circle represents naïve mice pre-infused with saline prior to Krystexxa dosing; solid blue square represents PEG-sensitized mice pre-infused with 40 kDa free PEG prior to Krystexxa dosing, and solid red triangle represents PEG-sensitized mice pre-infused with saline prior to Krystexxa dosing. Error bars represent standard deviation.

The amount of Krystexxa in the circulation in APA+, saline-treated mice continued to decline after the first four hours, and less than 5% of the injected dose remained in the circulation after 24 hrs (Figure 3.5A). Overall, the detectible levels of circulating Krystexxa in the four APA+ mice were 66%, 20%, 7%, and 4% of the average concentration seen in naïve mice at 24 hrs (Figure 3.5A), with a greater degree of reduction corresponding to a greater APA titer observed at baseline (3, 5, 24, 18 µg/mL respectively). APA-mediated clearance of Krystexxa resulted primarily in deposition in the liver, with nearly 60% of the injected dose found in the liver after 4 hrs, and ~80% after 24 hrs (Figure 3.5B). Due to the rapid hepatic accumulation in mice with APA at baseline who were not pre-treated with free PEG, less Krystexxa was found in both the kidneys and lungs at all times during the study in these animals (Figure 3.5C, D). APA

did not alter the amount of Krystexxa found in the muscles, with a very low intensity of Krystexxa-associated radioactivity in the observed section of muscle at all timepoints (Figure 3.5E).

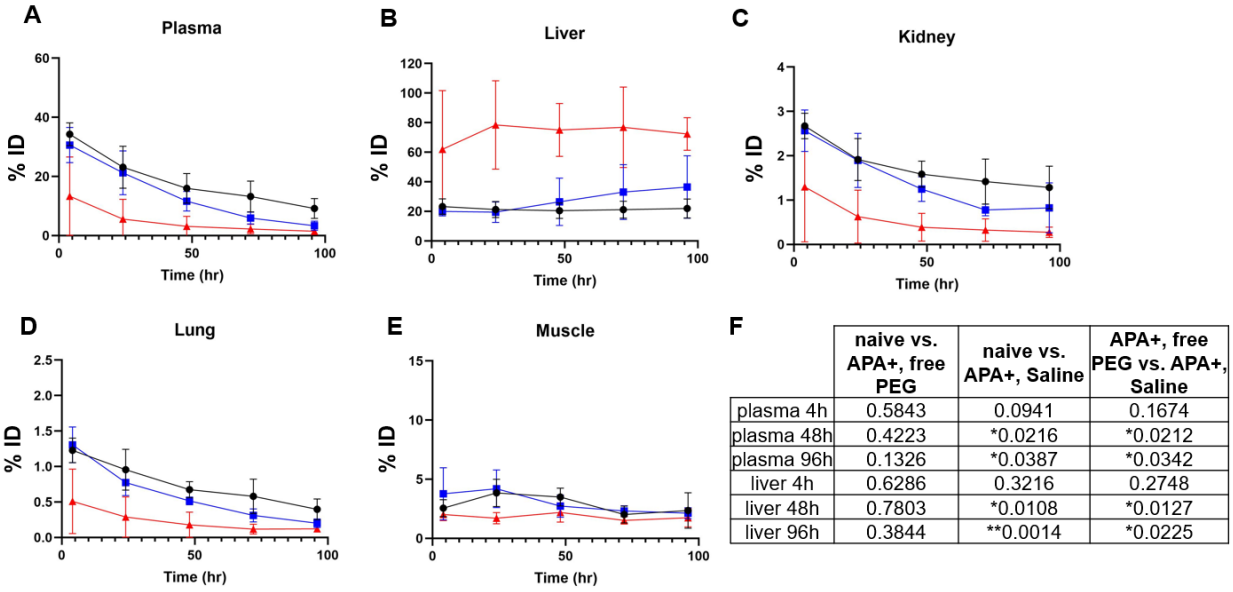

F

	naive vs. APA+, free PEG	naive vs. APA+, Saline	APA+, free PEG vs. APA+, Saline
plasma 4h	0.5843	0.0941	0.1674
plasma 48h	0.4223	*0.0216	*0.0212
plasma 96h	0.1326	*0.0387	*0.0342
liver 4h	0.6286	0.3216	0.2748
liver 48h	0.7803	*0.0108	*0.0127
liver 96h	0.3844	**0.0014	*0.0225

Figure 3.5. Mean Krystexxa Levels Through 96h. Mean Krystexxa levels over the first 96h in (A) plasma, (B) liver, (C) kidney, (D) lung, and (E) muscle, as determined by PET/CT imaging. Solid black circle represents naïve mice pre-infused with saline prior to Krystexxa dosing; solid blue square represents PEG-sensitized mice pre-infused with 40 kDa free PEG prior to Krystexxa dosing, and solid red triangle represents PEG-sensitized mice pre-infused with saline prior to Krystexxa dosing. Error bars represent standard deviation. (F) Multiple comparisons highlighting statistical differences (adjusted p-values) in key organs and time points. Plasma Krystexxa levels are not statistically different between the cohort treated with free PEG and the naïve mice through 96 hrs (Welch's ANOVA, Dunnett's T3 multiple comparisons). Liver uptake is not statistically between the free PEG-treated cohort and naïve cohort through 96 hrs, while both of these groups have significantly less liver accumulation than the untreated cohort at the 96 hrs time point (Welch's ANOVA and Dunnett's T3, $p < 0.05$). Likewise, the free PEG-treated and naïve cohorts do not statistically differ through 96 hrs in the kidney and lung, whereas the untreated cohort with APA has greater clearance at the earlier time points (Welch's ANOVA and Dunnett's T3, $p < 0.05$). Muscle Krystexxa levels do not significantly differ between cohorts (Welch's ANOVA).

After PET-imaging at 96 hrs, we sacrificed the mice, harvested the blood and organs, and assessed the amount of radioactivity in all tissues using a traditional gamma counter. The amount of Krystexxa remaining in the blood as well as the relative amounts in different organs (measured via gamma counter) were in good agreement with the amounts estimated based on PET/CT imaging. These results validated our use of PET/CT imaging to assess the real-time pharmacokinetic profile of Krystexxa in live animals.

Free PEG infusion restores prolonged circulation profile of Krystexxa and delays distribution to the liver

Unlike APA+ mice treated with saline, the amount of circulating Krystexxa in APA+ mice treated with free PEG was restored to nearly the same high concentrations seen in naïve mice over the first 48 hrs. Although apparent differences began to emerge at the 72 hrs and 96 hrs time points, with a relative decline in the free PEG-treated animals, this decline was not statistically significantly different from the animals without APA (applying Welch's ANOVA followed by Dunnett's T3 multiple comparisons test) (Figure 3.5A). The similar PK profiles were corroborated by a near-identical biodistribution profile seen between APA+, free PEG-treated mice vs. naïve mice over the first 48 hrs, with differences in amounts found in the liver, kidney and lung beginning to emerge only at the 72 hrs and 96 hrs time points (Figure 3.5B-D). The amount of Krystexxa found in the muscles was not statistically different from naïve mice or APA+, saline-treated mice at any of the later time points (Welch's ANOVA) (Figure 3.5E).

Based on the amounts of ^{89}Zr-Krystexxa detected in the blood and different organs over time, we calculated the AUC of Krystexxa in different organs over the first 96 hrs for the different treatment groups, which we used to compare the effectiveness of free PEG in restoring

the PK of Krystexxa. Compared to naïve mice, the presence of APA reduced the blood $AUC_{0\text{-}96h}$ of Krystexxa by over 70% (Figure 3.6A). In contrast, free PEG infusion mitigated much of that loss, with just a ~20% decline in $AUC_{0\text{-}96h}$ compared to naïve mice. Not surprisingly, very similar AUC values between naïve mice and APA+, free-PEG treated mice were found for all major organs, including the liver, kidney, lung, and muscle (Figure 3.6B, C). Given the good agreement between the estimations of circulating Krystexxa when measured by gamma counter or PET, we believe PET/CT provided an accurate estimate of the effectiveness of free PEG.

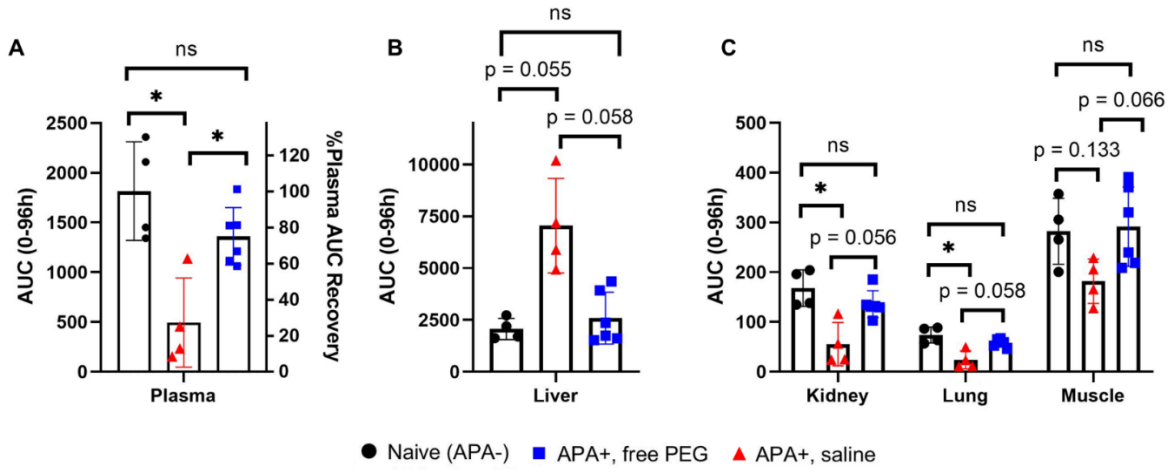

Figure 3.6. AUC and % AUC Recovered. AUC and % AUC recovered relative to naïve animals for (A) plasma, (B) liver, and (C) kidney, lung, and muscle. Error bars represent standard deviation. One-way ANOVA and multiple comparison testing (Kruskal-Wallis followed by Dunn's; Brown-Forsythe and Welch followed by Dunnett's T3) demonstrated a difference between the Naïve and APA+, saline cohorts (* $p < 0.05$), whereas the APA+, PEG cohort was not significantly different from Naïve. AUC in all organs in the free PEG-treated cohort is similar to AUC in the naïve cohort. Reported p-values are from Dunnett's T3 and have been adjusted for multiple comparisons. There is some overlap between the behavior of the mouse with low APA in the saline-treated cohort and the mice with high APA in the free PEG-treated cohort.

Increased APA levels correlate to faster elimination of Krystexxa from the circulation to the liver

We hypothesized that lower concentrations of APA at the time of administration of Krystexxa would lead to slower clearance of Krystexxa from the circulation, since lower APA levels should translate to either less APA bound to Krystexxa, or a longer duration before a critical threshold of bound APA is achieved. We thus compared the concentration of APA measured at Day 14 (~2-3 days prior to the PET/CT study) to the resulting PK profiles and biodistribution in mice. In good agreement with our expectation, the mice with lower APA titers had greater levels of Krystexxa detected in the circulation at all time points studied (Figure 3.7). Starting from 24 hrs post-administration, the amounts of ^{89}Zr-Krystexxa detected in the circulation in mice with ≥ 5 μg/mL IgG APA were cleared with virtually identical speed and to comparable extent, suggesting a critical threshold for APA in the clearance of Krystexxa. In contrast, with ≤ 2.5 μg/mL IgG APA, high to modest quantities of Krystexxa was detectable through the first 72 hrs. By the 96 hrs time point, the amount of Krystexxa in the circulation was effectively at background level regardless of the initial IgG APA levels in the PEG-sensitized mice (Figure 3.7C, D). Not surprisingly, we see a similar relationship between circulating APA levels and the amount of Krystexxa accumulated in the liver at different time points; mice possessing the highest APA titers also had the greatest fraction of injected dose of Krystexxa found in the liver, which became apparent as early as 24h.

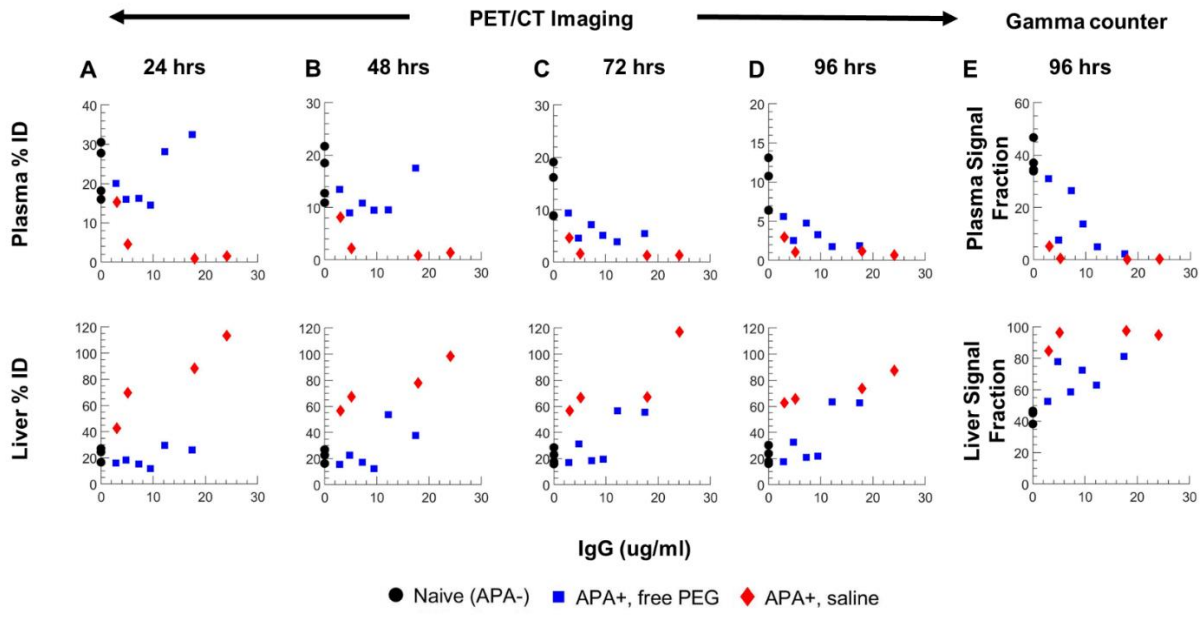

Figure 3.7. %ID as a function of APA. %ID of ^{89}Zr-Krystexxa signal in blood and liver as a function of IgG APA in serum, quantified by PET/CT imaging at (A) 24 hrs, (B) 48 hrs, (C) 72 hrs, and (D) 96 hrs post infusion. (E) Gamma counter measurements of radioactivity in excised organs at 96 hrs confirms the trends observed by PET/CT data.

Free PEG infusion is effective across a range of APA titers

At very high APA levels, it is mathematically more difficult for free PEG to saturate all circulating APA and competitively inhibit APA from binding and clearing Krystexxa from the circulation. We thus correlated the measured APA levels to the observed PK. At modest APA titers that led to rapid clearance of Krystexxa in placebo control mice, the infusion of free PEG afforded near-complete restoration of the Krystexxa PK and biodistribution profiles (Figure 3.7). Even at the highest APA titer (17 µg/mL), free PEG infusion restored ~60% of the AUC for levels of Krystexxa in the circulation. These results underscore the ability for free PEG infusion to overcome a range of APA titers to extend the circulation of PEG-uricase, allowing it to continue to reduce serum uric acid levels.

Discussion

As a result of the increasing number of PEGylated therapeutics authorized for human use, including the recent Pfizer/BioNTech and Moderna COVID mRNA vaccines, there has been increasing attention on the potential induction of APA, since APA may render select PEGylated therapies unsafe and/or not efficacious in some patients. For instance, Hershfield *et al.* found that over 60% of patients with APA experienced an adverse event after receiving pegloticase [3]. While Krystexxa is the foremost example for APA-induced loss of efficacy of a PEGylated drug, there are other PEGylated drugs whose efficacy are also impacted by APA. This includes Oncospar, a PEG-asparaginase used as part of frontline therapy for acute lymphoblastic leukemia in young children. The high failure to respond to Oncospar treatment, nearly 1 in 3, is strongly associated with the presence of APA [28, 34-36]. Evidence is emerging for other PEGylated drugs, including pegnivacogin, where acute severe allergic response is attributed to APA-mediated complement activation [37]. Thus, there is considerable urgency in developing interventions that could mitigate the loss of efficacy and increased incidence of adverse events due to APA.

While an array of new molecules is under active clinical development, given the exorbitant costs and long timelines in advancing new therapeutic molecules through clinical studies, it is far more attractive to develop an intervention that is PEG-specific, and can restore the efficacy of a multitude of PEGylated therapeutics. Here, building off of our recent work utilizing free PEG as a decoy that binds circulating APA and competitively inhibits APA from binding to PEG-liposomes, we evaluated whether a similar strategy could also effectively restore the prolonged circulation of Krystexxa. At low to moderate APA levels that are induced by Krystexxa, we showed that a simple prior infusion of free PEG was able to restore nearly 80% of

the AUC for amount of Krystexxa in the circulation of naïve mice, with virtually no difference in the PK and biodistribution profiles over the first 48 hrs. Even at the highest APA titers, free PEG infusion appeared to recover ~60% of the AUC. Based on allometric scaling of mouse to humans, we believe this effect is likely meaningful clinically: the half-life of Krystexxa in naïve mice from our study was ~30 hours, in good agreement with other studies [1, 38], whereas the median half-life of Krystexxa in patients is 214 hours, with the elimination likely driven by renal/urinary excretion [39]. In contrast, the half-life of Krystexxa in APA+ mice without free PEG intervention was ~12 hours. These results would suggest the free PEG intervention may restore the prolonged circulation of Krystexxa for many days in patients whose APA would otherwise quickly clear Krystexxa and render the treatment ineffective.

Our approach with using free PEG to specifically saturate APA contrasts with current approaches focused on broad immunosuppression. Broad immunosuppression can carry significant side effects [40]. For instance, treatment with mTOR inhibitor or methotrexate has been associated with increased risk of infection or sepsis [41-43]. Our approach also contrasts sharply with the use of alternative polymers to replace PEG. Although many alternatives to PEG are under active investigation [9, 10, 12, 44], it remains unclear if any will possess the same degree of safety in humans as PEG, or even if they would be less immunogenic. Furthermore, given the enormous costs to bring a new treatment to market and the large number of PEGylated drugs in clinical development, we believe the most cost effective and readily translatable approach is to specifically inhibit APA from binding to PEGylated drugs, rather than develop new substitutes for each impacted PEGylated drug.

Although it may seem paradoxical to overcome anti-PEG immunity by dosing in substantial doses of PEG, our approach is rooted in decades of prior studies that found PEG

immunogenicity to primarily result from grafting PEG to proteins or lipids, and that immunogenicity of the compounds is related to the immunogenicity of the proteins themselves [14, 22, 25, 28]. In other words, PEG may act as a hapten that elicits an immune response only when attached to a large carrier such as a protein or lipid drug carriers. A large number of preclinical studies have investigated the safety of infusing simply high MW PEG: beyond the occasional observation of benign PEG-related vacuolation in select tissues, the infusion of free PEG has generally been exceptionally safe [45], and no evidence of deposition of immune complexes in kidney that may lead to inflammation and glomerular disease [21, 46]. Thus, the infusion of free PEG effectively shifts the potential immunogenicity profile of a treatment, from the more immunogenic form of PEG associated with a protein or lipid, to the less immunogenic form of free PEG alone. It is certainly possible to saturate APA by simply dosing more PEGylated drugs. However, increasing the dose and/or adjusting the dosing frequency, particularly for drugs with dose-limited toxicity, is not only time-consuming but may yield unintended toxicities associated with the active molecule.

Based on the same principles of presenting PEG-decoys to saturate APA, one may obtain similar benefits of prolonging the systemic circulation of a PEGylated drug in APA+ animals by pretreating with empty PEG-liposomes. Indeed, Szebeni *et al.* elegantly showed that low-dose pre-infusion of Doxebo (empty PEG-liposomes) can block an anaphylactic response to subsequent doses of Doxil [47]. However, we believe free PEG offers unique advantages over PEG-liposomes. First, free PEG is far less immunostimulatory than PEG-liposomes, which can elicit much greater APA production [22, 24, 48, 49]. We can more readily achieve a substantial molar excess with free-PEG:APA than PEG-liposomes:APA; this in turn limits the formation of immune complexes with multiple anti-PEG B-cell receptors on APA-secreting B-cells, a

necessary event to stimulate B-cell expansion and APA secretion. Finally, no PEGylated intervention can be more cost-effective than free-PEG, since USP-grade PEG is readily available. All these factors contributed to our decision to pursue the use of free-PEG to overcome APA, rather than develop more complex interventions that may be scientifically novel but face significant developmental hurdles. Despite its simplicity, we found free PEG to limit short term APA induction to an extent not statistically different than PEG-liposomal doxorubicin (PL-dox) and rapamycin (PL-rapa) that directly kill or block proliferation of APA-specific B-cells, respectively [27]. Free PEG also appeared to provide long lasting suppression of APA induction (over 77 days), whereas PL-dox and PL-rapa both failed to provide meaningful suppression of APA induction beyond the first 21 days [27]. Coupled with our current results, we believe free PEG infusion appears to be a promising intervention to overcome APA-mediated clearance of PEGylated therapeutics.

Methods

Mouse model and induction of APA

Animal procedures used in this study were approved by the University of North Carolina at Chapel Hill's Institutional Animal Care and Use Committee. BALB/c mice aged 4-5 weeks were obtained from Charles River Labs and allowed to acclimate so that they would be young adults by the time of study. To account for potential sex differences, half the mice in each cohort were male and half were female. On Day 0, 10 mice were injected IV with 150 µL Krystexxa solution dosed at 0.9 mg/kg. This produced a controlled immune response study range through approximately 2-20 µg/mL anti-PEG IgG (Figure 3.3).

Collection of plasma for quantitating APA titers

At periodic time points (Day -1, Day 9, Day 14), mice were bled via mandibular bleed (200 µL whole blood). The blood was kept in EDTA tubes on ice. Samples were then centrifuged at 2000 rcf for 15 minutes and the plasma was stored at -80 ^{o}C. Samples were thawed and kept at 4 ^{o}C for short-term processing. All plasma samples were subjected to exactly 1 freeze-thaw cycle.

Measurements of anti-PEG IgG and IgM

Anti-PEG IgG and IgM levels were determined via competition ELISA based on previously established protocols [27]. 96-well plates were coated overnight at 4 ^{o}C with DSPE-PEG5000, and blocked with 5% milk in 1x PBS at room temperature for 1 hr. Plasma samples were diluted 50-fold in 1% milk with or without 8 kDa free PEG. Plates were incubated overnight at 4 ^{o}C, followed by washing. Then, goat anti-mouse IgG (Invitrogen, A28177, lot TG2596484) or IgM (ThermoFisher Life Technologies, 626820, lot QB215229) conjugated to HRP was added to the wells, incubated at room temperature for 1 hour, and washed. Finally, TMB was added to the wells, and after a waiting period, the conversion was stopped with 1N HCl. The plates were read at 450 and 570 nm, and 5-parameter logistic regression was performed on the standard curves. All individual specimens were measured in duplicate within an experiment, and 2 independent experiments were performed for all samples, with reported values an average of all measurements. All absorbance values, after subtracting the corresponding PEG-competition wells, were compared to APA isotype standards to determine the precise IgG and IgM APA in the specimens on a mass concentration basis. Standards were

made from mouse anti-PEG IgG (Silver Lake, CH2076, lot K0868) and IgM (Academia Sinica, AGP4 (AGP4-PABM-A)).

Radiolabeling of Krystexxa

Krystexxa was provided by Horizon Pharma and stored according to instructions until use. To radiolabel Krystexxa for PET imaging, we conjugated ~130 µg of Krystexxa via Df chelation (p-SCN-Bn-Deferoxamine, lot B70510004-150407) targeting free amine groups on available lysine. The Krystexxa-chelator conjugate was purified using a PD-10 column to remove unreacted chelator. The Df-Krystexxa was then labeled with ^{89}Zr in two batches [31]. The first batch produced 46% yield (3.5 mCi with 65 µg Df-Krystexxa, received 1.6 mCi), and the second batch produced 80% yield (1 mCi with 65 µg Df-Kryxtexxa, received 0.8 mCi). The samples were combined to form the solution dosed to the mice.

Mouse PET/CT Study

On Day 16/17, the mice were prepared for PET/CT imaging using a small animal PET/CT imaging system (SuperArgus 4R, Sedecal Inc., Spain). The APA+ mice were randomly divided into two groups (saline placebo control vs. free PEG treatment). A group of naïve Balb/c mice (i.e., not PEG-sensitized) was included as a negative control. A 1.5%-2.5% isoflurane-oxygen gas mixture was used to anesthetize the mice. All mice received either saline (for naïve group and placebo group) or 40 kDa free PEG (550 mg/kg) by slow infusion through tail vein catheter over 2 min. Group information was blinded to the animal treatment handler. Mice were then placed in a multi-animal imaging cradle in groups of 4 for simultaneous imaging. After 45

min, the mice received a bolus injection of ^{89}Zr-Krystexxa (4.1±1.3 MBq, equivalent to ~4.7 μg of Krystexxa in mass), followed immediately with dynamic PET scan for 60 mins. CT was conducted afterwards for anatomical reference. Repeated PET/CT scans were conducted at 4, 24, 48, 72, and 96 hours post injection of ^{89}Zr-Krystexxa. For the first 1-hour dynamic scan, images were binned into 19 frames with the following scheme: 6x10s, 4x30s, 2x60s, 3x300s, and 4x600s. The static scans at later time points were acquired for 20 minutes. 3D-OSEM algorithms with scatter, attenuation, and decay correction were used to reconstruct the PET images. For image analysis, PET and CT images were first registered and regions of interest (ROIs) were drawn in major organs for ROI-based PET image analysis. The standardized uptake value (SUV) and %ID/g were reported as the quantitative measure of the uptake level in each organ and tissue. %ID for each organ was further calculated by multiplying %ID/g with the estimated organ mass based on the empirical estimation [50-52]. All the analysis procedures were conducted using PMOD software (version 3.9). After the PET scan at 96 hrs, the mice were sacrificed. The liver, lung, spleen, kidney, and muscle tissue were harvested, as well as organs that did not account for substantial uptake including the heart and brain. Blood samples were centrifuged for separation into “plasma” and “blood cells and other sediments.” Heart and lung tissue were flushed with saline and dried with gauze before gamma counting. Gamma counter readings were performed on collected specimens to quantify ^{89}Zr activity.

Acknowledgments

We like to thank the staff at the UNC Animal Studies Core.

REFERENCES

[1] A.C. Nyborg, C. Ward, A. Zacco, B. Chacko, L. Grinberg, J.C. Geoghegan, R. Bean, M. Wendeler, F. Bartnik, E. O'Connor, F. Gruia, V. Iyer, H. Feng, V. Roy, M. Berge, J.N. Miner, D.M. Wilson, D. Zhou, S. Nicholson, C. Wilker, C.Y. Wu, S. Wilson, L. Jermutus, H. Wu, D.A. Owen, J. Osbourn, S. Coats, M. Baca, A Therapeutic Uricase with Reduced Immunogenicity Risk and Improved Development Properties, PLoS One, 11 (2016) e0167935.

[2] A. Guttmann, S. Krasnokutsky, M.H. Pillinger, A. Berhanu, Pegloticase in gout treatment - safety issues, latest evidence and clinical considerations, Therapeutic advances in drug safety, 8 (2017) 379-388.

[3] M.S. Hershfield, N.J. Ganson, S.J. Kelly, E.L. Scarlett, D.A. Jaggers, J.S. Sundy, Induced and pre-existing anti-polyethylene glycol antibody in a trial of every 3-week dosing of pegloticase for refractory gout, including in organ transplant recipients, Arthritis Research & Therapy, 16 (2014) R63.

[4] P.E. Lipsky, L.H. Calabrese, A. Kavanaugh, J.S. Sundy, D. Wright, M. Wolfson, M.A. Becker, Pegloticase immunogenicity: the relationship between efficacy and antibody development in patients treated for refractory chronic gout, Arthritis Research & Therapy, 16 (2014) R60.

[5] M.K. Reinders, T.L.T.A. Jansen, New advances in the treatment of gout: review of pegloticase, Ther Clin Risk Manag, 6 (2010) 543-550.

[6] J.S. Sundy, H.S.B. Baraf, R.A. Yood, N.L. Edwards, S.R. Gutierrez-Urena, E.L. Treadwell, J. Vázquez-Mellado, W.B. White, P.E. Lipsky, Z. Horowitz, W. Huang, A.N. Maroli, R.W. Waltrip, II, S.A. Hamburger, M.A. Becker, Efficacy and Tolerability of Pegloticase for the Treatment of Chronic Gout in Patients Refractory to Conventional Treatment: Two Randomized Controlled Trials, JAMA, 306 (2011) 711-720.

[7] W.M. Gentry, M.P. Dotson, B.S. Williams, M. Hartley, K.R. Stafford, M.B. Bottorff, P.K. Gandhi, Investigation of pegloticase-associated adverse events from a nationwide reporting system database, American Journal of Health-System Pharmacy, 71 (2014) 722-727.

[8] N.E. Elsadek, A.S. Abu Lila, T. Ishida, 5 - Immunological responses to PEGylated proteins: anti-PEG antibodies, in: G. Pasut, S. Zalipsky (Eds.) Polymer-Protein Conjugates, Elsevier, 2020, pp. 103-123.

[9] P. Zhang, F. Sun, C. Tsao, S. Liu, P. Jain, A. Sinclair, H.-C. Hung, T. Bai, K. Wu, S. Jiang, Zwitterionic gel encapsulation promotes protein stability, enhances pharmacokinetics, and reduces immunogenicity, Proc Natl Acad Sci U S A, 112 (2015) 12046-12051.

[10] K. Knop, R. Hoogenboom, D. Fischer, U.S. Schubert, Poly(ethylene glycol) in Drug Delivery: Pros and Cons as Well as Potential Alternatives, Angewandte Chemie International Edition, 49 (2010) 6288-6308.

[11] S. Abbina, A. Parambath, 14 - PEGylation and its alternatives: A summary, in: A. Parambath (Ed.) Engineering of Biomaterials for Drug Delivery Systems, Woodhead Publishing, 2018, pp. 363-376.

[12] Y. Qi, A. Chilkoti, Protein-Polymer Conjugation—Moving Beyond PEGylation, Current opinion in chemical biology, 28 (2015) 181-193.

[13] M. Barz, R. Luxenhofer, R. Zentel, M.J. Vicent, Overcoming the PEG-addiction: well-defined alternatives to PEG, from structure–property relationships to better defined therapeutics, Polymer Chemistry, 2 (2011) 1900-1918.

[14] B. Li, Z. Yuan, H.-C. Hung, J. Ma, P. Jain, C. Tsao, J. Xie, P. Zhang, X. Lin, K. Wu, S. Jiang, Revealing the Immunogenic Risk of Polymers, Angewandte Chemie International Edition, 57 (2018) 13873-13876.

[15] S.B. van Witteloostuijn, S.L. Pedersen, K.J. Jensen, Half-Life Extension of Biopharmaceuticals using Chemical Methods: Alternatives to PEGylation, ChemMedChem, 11 (2016) 2474-2495.

[16] P. Zhang, P. Jain, C. Tsao, K. Wu, S. Jiang, Proactively Reducing Anti-Drug Antibodies via Immunomodulatory Bioconjugation, Angewandte Chemie International Edition, 58 (2019) 2433-2436.

[17] T.K. Kishimoto, J.D. Ferrari, R.A. LaMothe, P.N. Kolte, A.P. Griset, C. O'Neil, V. Chan, E. Browning, A. Chalishazar, W. Kuhlman, F.-n. Fu, N. Viseux, D.H. Altreuter, L. Johnston, R.A. Maldonado, Improving the efficacy and safety of biologic drugs with tolerogenic nanoparticles, Nature Nanotechnology, 11 (2016) 890-899.

[18] C.P. Carpenter, M.D. Woodside, E.R. Kinkead, J.M. King, L.J. Sullivan, Response of dogs to repeated intravenous injection of polyethylene glycol 4000 with notes on excretion and sensitization, Toxicology and applied pharmacology, 18 (1971) 35-40.

[19] H.F. Smyth, Jr., C.P. Carpenter, C.B. Shaffer, The toxicity of high molecular weight polyethylene glycols; chronic oral and parenteral administration, Journal of the American Pharmaceutical Association. American Pharmaceutical Association, 36 (1947) 157-160.

[20] R. Stidl, S. Fuchs, M. Bossard, J. Siekmann, P.L. Turecek, M. Putz, Safety of PEGylated recombinant human full-length coagulation factor VIII (BAX 855) in the overall context of PEG and PEG conjugates, Haemophilia, 22 (2016) 54-64.

[21] R. Webster, V. Elliott, B.K. Park, D. Walker, M. Hankin, P. Taupin, PEG and PEG conjugates toxicity: towards an understanding of the toxicity of PEG and its relevance to PEGylated biologicals, in: F.M. Veronese (Ed.) PEGylated Protein Drugs: Basic Science and Clinical Applications, Birkhäuser Basel, Basel, 2009, pp. 127-146.

[22] Y. Mima, Y. Hashimoto, T. Shimizu, H. Kiwada, T. Ishida, Anti-PEG IgM Is a Major Contributor to the Accelerated Blood Clearance of Polyethylene Glycol-Conjugated Protein, Molecular pharmaceutics, 12 (2015) 2429-2435.

[23] A.W. Richter, E. Åkerblom, Antibodies against Polyethylene Glycol Produced in Animals by Immunization with Monomethoxy Polyethylene Glycol Modified Proteins, International Archives of Allergy and Immunology, 70 (1983) 124-131.

[24] T. Ishida, X. Wang, T. Shimizu, K. Nawata, H. Kiwada, PEGylated liposomes elicit an anti-PEG IgM response in a T cell-independent manner, Journal of Controlled Release, 122 (2007) 349-355.

[25] X. Wan, J. Zhang, W. Yu, L. Shen, S. Ji, T. Hu, Effect of protein immunogenicity and PEG size and branching on the anti-PEG immune response to PEGylated proteins, Process Biochemistry, 52 (2017) 183-191.

[26] M.D. McSweeney, L.S.L. Price, T. Wessler, E.C. Ciociola, L.B. Herity, J.A. Piscitelli, A.C. DeWalle, T.N. Harris, A.K.P. Chan, R.S. Saw, P. Hu, J.C. Jennette, M.G. Forest, Y. Cao, S.A. Montgomery, W.C. Zamboni, S.K. Lai, Overcoming anti-PEG antibody mediated accelerated blood clearance of PEGylated liposomes by pre-infusion with high molecular weight free PEG, Journal of Controlled Release, 311-312 (2019) 138-146.

[27] M.D. McSweeney, L. Shen, A.C. DeWalle, J.B. Joiner, E.C. Ciociola, D. Raghuwanshi, M.S. Macauley, S.K. Lai, Pre-treatment with high molecular weight free PEG effectively suppresses anti-PEG antibody induction by PEG-liposomes in mice, Journal of Controlled Release, (2020).

[28] P. Zhang, F. Sun, S. Liu, S. Jiang, Anti-PEG antibodies in the clinic: Current issues and beyond PEGylation, Journal of Controlled Release, 244 (2016) 184-193.

[29] Q. Yang, T.M. Jacobs, J.D. McCallen, D.T. Moore, J.T. Huckaby, J.N. Edelstein, S.K. Lai, Analysis of Pre-existing IgG and IgM Antibodies against Polyethylene Glycol (PEG) in the General Population, Analytical Chemistry, 88 (2016) 11804-11812.

[30] M.D. McSweeney, T. Wessler, L.S.L. Price, E.C. Ciociola, L.B. Herity, J.A. Piscitelli, W.C. Zamboni, M.G. Forest, Y. Cao, S.K. Lai, A minimal physiologically based pharmacokinetic model that predicts anti-PEG IgG-mediated clearance of PEGylated drugs in human and mouse, Journal of Controlled Release, 284 (2018) 171-178.

[31] M.J.W.D. Vosjan, L.R. Perk, G.W.M. Visser, M. Budde, P. Jurek, G.E. Kiefer, G.A.M.S. van Dongen, Conjugation and radiolabeling of monoclonal antibodies with zirconium-89 for PET imaging using the bifunctional chelate p-isothiocyanatobenzyl-desferrioxamine, Nature Protocols, 5 (2010) 739-743.

[32] L.P. Ganesan, Y. Kim J Fau - Wu, S. Wu Y Fau - Mohanty, G.S. Mohanty S Fau - Phillips, D.J. Phillips Gs Fau - Birmingham, J.M. Birmingham Dj Fau - Robinson, C.L. Robinson Jm Fau - Anderson, C.L. Anderson, FcγRIIb on liver sinusoidal endothelium clears small immune complexes.

[33] O.M. Merkel, R. Urbanics, P. Bedőcs, Z. Rozsnyay, L. Rosivall, M. Toth, T. Kissel, J. Szebeni, In vitro and in vivo complement activation and related anaphylactic effects associated with polyethylenimine and polyethylenimine-graft-poly(ethylene glycol) block copolymers, Biomaterials, 32 (2011) 4936-4942.

[34] J.K. Armstrong, G. Hempel, S. Koling, L.S. Chan, T. Fisher, H.J. Meiselman, G. Garratty, Antibody against poly(ethylene glycol) adversely affects PEG-asparaginase therapy in acute lymphoblastic leukemia patients, Cancer, 110 (2007) 103-111.

[35] R. Kloos, I.M. van der Sluis, E. Mastrobattista, W. Hennink, R. Pieters, J.-J. Verhoef, Acute lymphoblastic leukaemia patients treated with PEGasparaginase develop antibodies to PEG and the succinate linker, British Journal of Haematology, 189 (2020) 442-451.

[36] Y. Liu, C.A. Smith, J.C. Panetta, W. Yang, L.E. Thompson, J.P. Counts, A.R. Molinelli, D. Pei, N.M. Kornegay, K.R. Crews, H. Swanson, C. Cheng, S.E. Karol, W.E. Evans, H. Inaba, C.H. Pui, S. Jeha, M.V. Relling, Antibodies Predict Pegaspargase Allergic Reactions and Failure of Rechallenge, Journal of clinical oncology : official journal of the American Society of Clinical Oncology, 37 (2019) 2051-2061.

[37] T.J. Povsic, M.G. Lawrence, A.M. Lincoff, R. Mehran, C.P. Rusconi, S.L. Zelenkofske, Z. Huang, J. Sailstad, P.W. Armstrong, P.G. Steg, C. Bode, R.C. Becker, J.H. Alexander, N.F. Adkinson, A.I. Levinson, Pre-existing anti-PEG antibodies are associated with severe immediate allergic reactions to pegnivacogin, a PEGylated aptamer, Journal of Allergy and Clinical Immunology, 138 (2016) 1712-1715.

[38] J.S. Bomalaski, F.W. Holtsberg, C.M. Ensor, M.A. Clark, Uricase formulated with polyethylene glycol (uricase-PEG 20): biochemical rationale and preclinical studies, The Journal of Rheumatology, 29 (2002) 1942.

[39] Product Information Annex: KRYSTEXXA 8 mg concentrate for solution for infusion, in: Product Information, European Medicines Agency, European Public Assessment Report, pp. 1-27.

[40] J. Youssef, S.A. Novosad, K.L. Winthrop, Infection Risk and Safety of Corticosteroid Use, Rheumatic diseases clinics of North America, 42 (2016) 157-x.

[41] G. Shi, S. Ozog, B.E. Torbett, A.A. Compton, mTOR inhibitors lower an intrinsic barrier to virus infection mediated by IFITM3, Proc Natl Acad Sci U S A, 115 (2018) E10069-e10078.

[42] A. Fisher, J.M. Seguel, A.N. de la Torre, D. Wilson, A. Merchant, R.K. Arora, B. Koneru, Effect of sirolimus on infection incidence in liver transplant recipients, Liver transplantation : official publication of the American Association for the Study of Liver Diseases and the International Liver Transplantation Society, 10 (2004) 193-198.

[43] A.M. Boerbooms, P.J. Kerstens, J.W. van Loenhout, J. Mulder, L.B. van de Putte, Infections during low-dose methotrexate treatment in rheumatoid arthritis, Seminars in arthritis and rheumatism, 24 (1995) 411-421.

[44] M. Barz, R. Luxenhofer, R. Zentel, M.J. Vicent, Overcoming the PEG-addiction: well-defined alternatives to PEG, from structure-property relationships to better defined therapeutics, Polymer Chemistry, 2 (2011) 1900-1918.

[45] I.A. Ivens, W. Achanzar, A. Baumann, A. Brändli-Baiocco, J. Cavagnaro, M. Dempster, B.O. Depelchin, A.R. Irizarry Rovira, L. Dill-Morton, J.H. Lane, B.M. Reipert, T. Salcedo, B. Schweighardt, L.S. Tsuruda, P.L. Turecek, J. Sims, PEGylated Biopharmaceuticals: Current Experience and Considerations for Nonclinical Development, Toxicologic pathology, 43 (2015) 959-983.

[46] A. Bendele, J. Seely, C. Richey, G. Sennello, G. Shopp, Short Communication: Renal Tubular Vacuolation in Animals Treated with Polyethylene-Glycol-Conjugated Proteins, Toxicological Sciences, 42 (1998) 152-157.

[47] Y. Bavli, I. Winkler, B.M. Chen, S. Roffler, R. Cohen, J. Szebeni, Y. Barenholz, Doxebo (doxorubicin-free Doxil-like liposomes) is safe to use as a pre-treatment to prevent infusion

reactions to PEGylated nanodrugs, Journal of controlled release : official journal of the Controlled Release Society, 306 (2019) 138-148.

[48] T. Ishida, H. Kiwada, [Accelerated blood clearance (ABC) phenomenon induced by administration of PEGylated liposome], Yakugaku zasshi : Journal of the Pharmaceutical Society of Japan, 128 (2008) 233-243.

[49] X. Wang, T. Ishida, H. Kiwada, Anti-PEG IgM elicited by injection of liposomes is involved in the enhanced blood clearance of a subsequent dose of PEGylated liposomes, Journal of controlled release : official journal of the Controlled Release Society, 119 (2007) 236-244.

[50] B. Davies, T. Morris, Physiological Parameters in Laboratory Animals and Humans, Pharmaceutical Research, 10 (1993) 1093-1095.

[51] R.P. Brown, M.D. Delp, S.L. Lindstedt, L.R. Rhomberg, R.P. Beliles, Physiological parameter values for physiologically based pharmacokinetic models, Toxicology and industrial health, 13 (1997) 407-484.

[52] N. Kaliss, D. Pressman, Plasma and blood volumes of mouse organs, as determined with radioactive iodoproteins, Proceedings of the Society for Experimental Biology and Medicine. Society for Experimental Biology and Medicine (New York, N.Y.), 75 (1950) 16-20.

CONCLUSION

The 8-compartment PBPK model, presented in this thesis, combined with experimentation, demonstrates the potential to predict the extent of and the mechanisms behind APA-mediated ABC. Furthermore, the results suggest free PEG intervention as a promising strategy to alleviate the altered PK as a result of ABC, restoring the biodistribution of a PEGylated therapeutic to trends comparable to the naïve cohort even in mice with moderately high APA titers. Increasing a drug's plasma circulation time increases the potential for the drug to be effective. Hence, implementing such a strategy would be invaluable for improving the accessibility of PEGylated drugs for patients who could greatly benefit from the treatments but are unable to tolerate them due to APA-related adverse reactions.

Future work involves expanding the multi-compartment PBPK model to account for the differential binding of anti-PEG IgG and anti-PEG IgM, as well as explicitly incorporating the competition behavior between free PEG and the PEGylated drug carriers as the IgG and IgM bind to and clear both PEGylated species. Continuing to expand on this model introduces the potential to predict a more efficient dosing regimen for free PEG – for example, whether it can be pre-mixed with the drug, whether a lower dose of PEG will produce comparable PK trends, or whether we can expect to see even greater improvement from the intervention at high APA titers. The model predictions for the effect of PEG dosing, combined with experimental data, will allow us to assess the costs and benefits of reducing the amount of free PEG injected. The goal is to optimize the strategy so that the patient could reap the benefits of the intervention (maximize

circulation of Krystexxa) without the need to inject extraneous PEG (minimize the dose of free PEG).

Future experimental projects aim to address whether the PK trends observed for Krystexxa hold in a setting more closely designed to simulate clinical treatment, i.e., after repeated dosing at 2-week intervals. In observing the biodistribution of a dose of radiolabeled Krystexxa at the end of 2 months, in addition to our detailed characterization of the second dose PK at the 2-week timepoint, we can infer a greater sense of how APA induced over time affect the biodistribution of Krystexxa in a population receiving the treatment at regular intervals. Thus, we can infer how PK (and by extension efficacy) can be altered over the duration of treatment.

Finally, scaling up to larger animal studies is the next step in working towards the translational implications of our PEG research. A swine model exhibits an anaphylactic response more similar to that of humans than the initial mouse model. Therefore, it is a suitable model for testing and confirming that (1) the free PEG itself is not immunogenic, (2) free PEG restores Krystexxa circulation to naïve-like levels in the plasma, and (3) free PEG holds the potential to suppress anaphylaxis as well as restore the PK profile. Demonstrating this would confirm a valuable strategy to increase the efficacy and mitigate the risk of PEGylated drugs in patients with APA.

As this work progresses, we will continue to leverage the intersection of PBPK model predictions and experimental data in the process of scaling up to develop an intervention for APA-mediated ABC with clinical potential.